Highlights

- The KRI3 peptide is a previously identified positively charged Ship2-Sam ligand.
- Cyclic and linear KRI3 analogues were evaluated via a multidisciplinary approach.
- Tyrosine residues in KRI3 are important for binding to Ship2-Sam.
- Cyclic KRI3 has higher serum stability than KRI3 but worse cellular uptake in PC3.
- KRI3 cellular uptake occurs without conjugation to cell penetrating cargo.

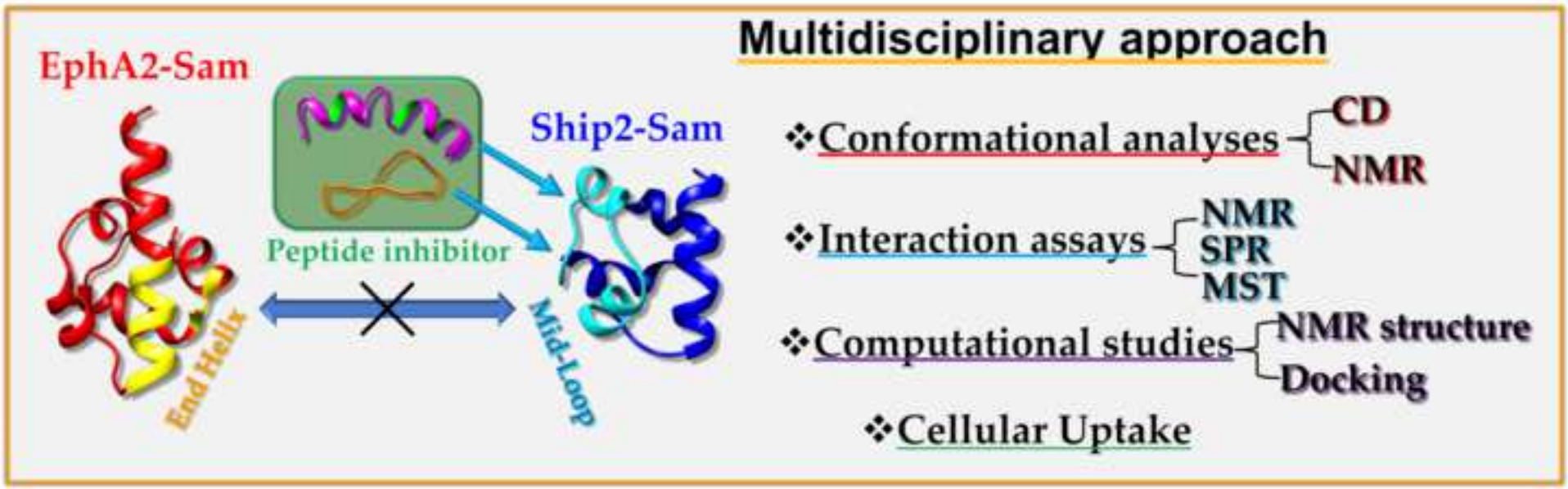

Targeting Ship2-Sam with peptide ligands: novel insights from a multidisciplinary approach

Marian Vincenzi[1@], Flavia Anna Mercurio[1@], Concetta Di Natale[2,3], Rosanna Palumbo[1], Luciano Pirone[1,5], Sara La Manna[4,5], Daniela Marasco[4,5], Emilia Maria Pedone[1,5], and Marilisa Leone[1,5*]

1 Institute of Biostructures and Bioimaging (CNR), Naples, Italy

2 Istituto Italiano di Tecnologia, IIT@CRIB, Naples, Italy

3 Centro di Ricerca Interdipartimentale sui Biomateriali CRIB, University of Naples Federico II, Naples, Italy

4 University of Naples Federico II, Department of Pharmacy, Naples, Italy

5 InterUniversity Research Centre on Bioactive Peptides (CIRPEB), University of Naples Federico II, Naples, Italy

*To whom correspondence should be addressed: Dr. Marilisa Leone. Institute of Biostructures and Bioimaging (CNR), Via Mezzocannone 16, 80134, Naples, Italy. Phone: +39(081) 2534512. Fax: +39(081) 2536642. E-mail: marilisa.leone@cnr.it.

@These authors contributed equally to this work

Keywords: SAM domains, EphA2, Ship2, cancer, NMR, SPR, MST, docking, cellular uptake.

Abstract

The lipid phosphatase Ship2 binds the EphA2 receptor through a heterotypic Sam-Sam (Sterile alpha motif) interaction. Inhibitors of the Ship2-Sam/EphA2-Sam complex hold a certain potential as novel anticancer agents. The previously reported "KRI3" peptide binds Ship2-Sam working as a weak antagonist of the EphA2-Sam/Ship2-Sam interaction. Herein, the design and functional evaluation of KRI3 analogues, both linear and cyclic, are described. A multidisciplinary study was conducted through computational docking techniques, and conformational analyses by CD and NMR spectroscopies. The ability of new peptides to bind Ship2-Sam was analysed by NMR, MST and SPR assays. Studies on linear KRI3 analogues pointed out that aromatic interactions through tyrosines are important for the association with Ship2-Sam whereas, an increase of the net positive charge of the sequence or peptide cyclization through a disulfide bridge can favour unspecific interactions without a substantial improvement of the binding affinity to Ship2-Sam. Interestingly, preliminary cell-based assays demonstrated KRI3 cellular uptake even without the conjugation to a cell penetrating sequence with a main cytosolic localization. This work highlights important features of the KRI3 peptide that can be further exploited to design analogues able to hamper Sam-Sam interactions driven by electrostatic contacts.

1. Introduction

Ship2 (Src homology 2 domain-containing inositol 5'-phosphatase 2) is a lipid phosphatase belonging to the 5'-phosphatases enzyme family [1]. It catalyzes mainly conversion of PIP3 (phosphatidylinositol 3,4,5-triphosphate) in phosphatidylinositol (3,4) P2 and consequently, induces downregulation of different PI3K (Phosphatidyl-Inositol 3 Kinase) activated pathways. Ship2 has several protein interactors and plays roles in physiological and pathological events [2]. For instance it is involved in actin cytoskeletal reorganization, receptor internalization, cell adhesion and spreading [1]. Ship2 regulates insulin sensitivity and obesity and represents a prominent target in drug discovery for type 2 diabetes. In addition, a connection has been established between Ship2 and other diseases

including opsismodysplasia (i.e., a pathology affecting bone development), atherosclerosis, and cancer [1]. The role of Ship2 in cancer is somehow controversial as it can play pro- and anti-tumorigenic functions based on the cell model [2]. Interestingly, Ship2 contains within its modular domain organization a Sam (Sterile alpha motif) domain (Fig. 1) [3]. Sam domains represent small protein binding modules made up of roughly 70 amino acids that fold in a five helix bundle [4]. The Sam domain of Ship2 (Ship2-Sam) is able to associate with the Sam domain of the EphA2-receptor (EphA2-Sam) [5] and the Sam domain of the PI3K effector protein Arap3 (Arap3-Sam) [6]. NMR and molecular modeling studies indicated that Ship2-Sam binds both EphA2-Sam and Arap3-Sam by forming heterodimers with identical interaction topologies [7-9].

Biophysical studies showed low micromolar dissociation constants for these heterotypic Sam-Sam interactions [8, 9]. In detail, Ship2-Sam binds the partner Sam domains through the canonical Mid-Loop (ML)/End Helix (EH) model of Sam-Sam complexes in which Ship2-Sam central region forms the so called ML Interface (Fig. 1) while the EH Interface is provided by part of the C-terminal α5 helices and close α1α2 loops in either EphA2-Sam and Arap3-Sam [7-9].

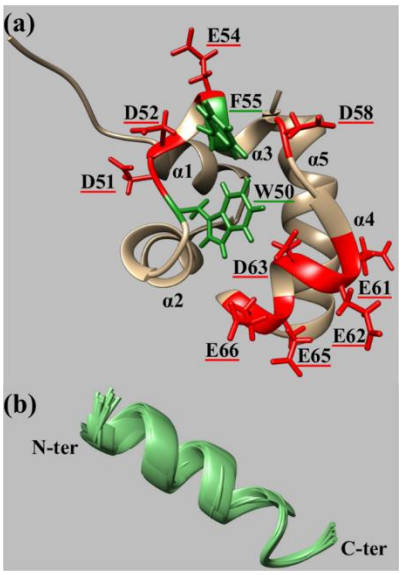

Fig. 1: (**a**) NMR solution structure of Ship2-Sam (pdb code: 2K4P [8], conformer n.1) in a ribbon representation, negatively charged and aromatic residues within the ML Interface are shown in red and green, respectively and labeled with the one letter amino acid codes and sequence numbers. (**b**) NMR solution structure of KRI3 peptide (PBS/TFE 50/50 v/v) in a ribbon representation. Twenty conformers are overlayed on the backbone atoms.

These Sam-Sam interactions are highly driven by electrostatic contacts as the ML Interface in Ship2-Sam is negatively charged whereas, the EH Interfaces in both Arap3-Sam and EphA2-Sam are positively charged; in addition, a few aromatic residues on both surfaces may contribute additional intermolecular contacts (Fig. 1) [7-9]. The functional role and the cellular pathways of the interaction between Ship2-Sam and Arap3-Sam have not been fully clarified whereas, more studies concerning the Ship2-Sam/EphA2-Sam association have been reported [5, 7].

EphA2 is a tyrosine kinase receptor that represents a critical player in cancer where it exhibits a debated role whose outcomes depend by a fine tuning of a ligand-dependent pro-oncogenic and a ligand independent anti-oncogenic route [10]. EphA2 receptor over-expression has been observed in many solid tumors - like ovarian, lung, pancreatic, breast, prostate cancers, and melanoma [11].

In malignant MDA-MB-231 breast cancer cells Ship2 inhibits EphA2 receptor endocytosis and consequently, Ship2 silencing enhances receptor internalization and degradation upon stimulation with an ephrin ligand [5]. To play this function Ship2 needs to be engaged at the receptor through the Ship2-Sam/EphA2-Sam association although also the catalytic activity of Ship2 is required [5].

In our laboratory we have long been focused on the Sam domain of the receptor (EphA2-Sam) to develop inhibitors of its heterotypic interactions with Ship2-Sam and the first Sam domain of the protein Odin (Odin-Sam1) [12]. Ship2 inhibits receptor endocytosis and consequent degradation [5] whereas, Sam domains of the protein Odin are important to enhance receptor stability likely through inhibition of ubiquitination [13]. To achieve our goal, we set up a variety of approaches to design peptide ligands of ML and EH surfaces [14-17]: sequences enriched in charged and helix promoting residues [18], stapled [19] and head to tail cyclic [20] peptides. Interestingly, through a protein dissection approach focused on EphA2-Sam we generated the KRI3 peptide (Table 1) [14]. This sequence, that targets the ML interface of Ship2-Sam, contains the -KRIAY- motif, located into the C-terminal helix in the EH site of EphA2-Sam (aa 956-960 in human EphA2 (Uniprot code P29317)) repeated thrice in tandem [14]. KRI3 was conceived considering that the binding site of Ship2-Sam

for EphA2-Sam is negatively charged and also contains a few aromatic residues (a phenylalanine and a tryptophan) (Fig. 1) and thus, the positive Lys and Arg residues along with the aromatic Tyr could provide several favorable intermolecular contacts [14]. KRI3 interacts with Ship2-Sam with a dissociation constant K_D~100 μM (in SPR (Surface Plasmon Resonance) experiments) and is a weak antagonist of the EphA2-Sam/Ship2-Sam association. NMR (Nuclear Magnetic Resonance) experiments in aqueous solution containing 50% 2,2,2-trifluoroethanol (TFE) provided a structure with an extended helical conformation (Fig. 1(**b**)) [14]. Noticeably, conjugated to Tat-derived cell penetrating peptide (CPP) KRI3 peptide induces necrosis in the PC-3 prostate cancer cell line and is more cytotoxic in cancer cells with respect to normal dermal fibroblasts [14].

With this in mind, starting from the KRI3 sequence, herein we designed and analyzed different linear and cyclic analogues (Table 1).

Table 1: Peptide sequences analyzed in the manuscript. Residues in common with KRI3 sequence are coloured red. Mutated amino acids in KRI3-IM and KRI3-YM are highlighted in blue together with the additional KRIAY motif in KRI4.

Peptide	Sequences
KRI3	Ac-KRIAYKRIAYKRIAY-NH_2
KRI3-YM	Ac-KRIA**A**KRIA**A**KRIA**A**-NH_2
KRI3-IM	Ac-KR**K**AYKR**K**AYKR**K**AY-NH_2
KRI4	Ac-KRIAYKRIAYKRIAY**KRIAY**-NH_2
cKRI3	CKRIAYKRIAYKRIAYC
Ac-cKRI3-NH_2	Ac-CKRIAYKRIAYKRIAYC-NH_2
Ac-cKRI3	Ac-CKRIAYKRIAYKRIAYC
cKRI3-NH_2	CKRIAYKRIAYKRIAYC-NH_2

Ac=N-terminal acetylation, NH_2=C-terminal amidation.

To study this novel peptide series against Ship2-Sam, we performed a multidisciplinary analysis made up of computational and experimental techniques including docking studies, conformational analyses, *in vitro* binding assays through NMR, MST (MicroScale Thermophoresis) and SPR. In addition, we evaluated the cellular localization of KRI3 and a few of its analogues to compare the effects of introduced chemical modifications.

2. Results and Discussion

2.1. Peptide design

Docking studies were conducted with Haddock [21] to get models of the Ship2-Sam/KRI3 complex. The protein docking site was set in the ML surface of Ship2-Sam following analysis of CSP (Chemical Shift Perturbation) data [14] and intensity changes of peaks in the [^{1}H, ^{15}N] spectrum of the protein upon addition of the KRI3 peptide (Supplementary Material - Fig. S1). For such studies the NMR structure of KRI3 calculated in solution containing 50% TFE was implemented [14] (Supplementary Material - Fig. S2). As evaluable from Fig. S2, a helical KRI3 peptide can be well located inside the ML interface of Ship2-Sam establishing multiple contacts (Supplementary Material - Table S1). In detail, the central -KRIAY- motif provides the largest number of interactions; in general, the positive lysines and arginines are responsible for a wide number of intermolecular interactions with the ML interface (1237 and 1345, respectively) along with the tyrosines (number of provided interactions equal to 1369). This is due to the negative and aromatic nature of the ML interface of Ship2-Sam (Fig. 1) [8]. To validate docking results a series of new analogues were designed and their sequences are reported in Table 1. Since Tyr appeared important for the interaction, we designed the KRI3-YM peptide, as negative control, bearing the mutation Tyr/Ala. Instead from docking studies Ile and Ala residues, appeared less involved into the interaction with the protein (providing 909 and 631 intermolecular contacts, respectively), hence, we designed the peptide KRI3-IM where the isoleucines were replaced by lysines to enhance electrostatic interactions. Similarly, the peptide KRI4 was conceived with four “KRIAY” stretches repeated in tandem to evaluate the effects of one additional consensus motif. We also designed cyclic cKRI3 analogues (Table 1) in which two cysteine residues were added at the N- and C-termini of the KRI3 sequence and cyclization was achieved through intramolecular disulfide bond formation. In this context, we focused on cKRI3 compounds bearing or not protections at the N- and C-terminal ends as additional modulating factors of the peptide charge for the interaction with Ship2-Sam (Table 1).

2.2. Conformational analysis

To investigate the conformational properties of designed KRI3 peptide analogues, we conducted structural analyses in solution by means of CD and NMR spectroscopy. 2D [^{1}H, ^{1}H] NMR spectra were recorded in aqueous buffer and in the presence of the structuring co-solvent TFE [22]. Short peptides are often flexible and disordered in a merely aqueous environment but TFE is very useful to unveil the conformational tendencies that could characterize their bioactive conformations [22]. CD studies were as well conducted under similar experimental conditions and during time.

2.2.1. CD investigations

Firstly, CD spectra were recorded in H_2O and aqueous sodium phosphate buffer at pH 7.2, at the indicated concentrations of TFE (Fig. 2 and Supplementary Material -Fig.s S3-S9). The overlays of CD spectra of cKRI3, Ac-cKRI3-NH_2 and cKRI3-NH_2 indicate similar conformational behaviors both in buffer (Fig.s 2(**a-c**), Supplementary Material -Fig.s S3-S5(**b**)) and in water (Supplementary Material -Fig.s S3-S5(**a**)). The deconvolutions of CD spectra were also performed (Supplementary Material -Tables S2-S4) [23]. In absence of TFE, mixed random-beta conformations can be detected for the presence of a minimum at ~ 218 nm and a negative band under 200 nm, for cKRI3 (Fig.2(**a**)) and Ac-cKRI3-NH_2 (Fig.2(**b)**). The addition of TFE leads to a more structured conformation both at 30 and 50% of TFE: in the spectra (Fig.s 2(**a-c**)) we observe a coalescence of initial minima in a broad band centered at 218 nm. As general feature, it is difficult to follow TFE-titration with non-canonical CD profiles. In addition, the absence of an isodichroic wavelength, during TFE titration, indicates the coexistence of different equilibria in solution and not a simple two-state mechanism of transition random coil to helix [24]. Further increase of TFE (70%) induces a major helical content for the clear distinction of two minima at 208 and 218 nm (Fig.s 2(**a-c**)). CD analysis during time (t=0, 24h) does not point out relevant conformational changes (Fig.s 2(**a-c**), Supplementary Material -Fig.s S3-S5(**a** left panel) for t=0; -Fig.s S3-S5(**a** right panel, **b**) for t=24 h). Deconvolution indicates that the contribution of uncanonical secondary structures is always prevalent even if the increase of

TFE partially stabilizes β-structures till ~ 30%, then, an enhancement of helical content is also estimated (Supplementary Material -Tables S2-S4). For Ac-cKRI3 sequence, at 0% TFE a major random content is evident, by raising TFE percentages an α-helical content can be also detected (Fig.s 2(**d**) and S6(**a** left panel)) and, similarly to other sequences, no conformational changes were evident after 24h (Supplementary Material -Fig.s S6(**a** right panel, **b**)). An extensive TFE titration suggests that the β content is still prevalent with respect to the helical one even at very high TFE amounts (50%) (Supplementary Material -Table S5). Similarly KRI3-IM at 0% TFE exhibits a typical disordered spectrum with a progressive enhancement of helical content at high percentages of TFE (Fig.s 2(**e**), S7(**b**), Table S6(**c,d**)). In this latter caseTFE titration does not reach saturated ellipticity intensity till 70% (v/v).

Also, KRI3-YM (Fig.s 2(**f**), S8) and KRI4 (Fig.s 2(**g**), S9) at 0% TFE exhibit typical random spectra that tend to assume more helical conformations at increasing amounts of TFE (Supplementary Material -Tables S7-S8). No relevant differences during time can be evidenced for both peptides (Supplementary Material -Table S7-S8).

The analysis of Θ_{min}, that is the Θ value at the relative minimum around the wavelength of 222 nm, vs TFE percentages (Supplementary Material -Fig. S10), indicates that for almost all sequences the highest value is reached at 50% of TFE (Fig.s S10(**a-c**),(**f-g**)) except for KRI3-IM peptide whose plateau is reached at 70 % of TFE (Fig. S10(**e**)) and Ac-cKRI3 that did not exhibit saturation (Fig. S10(**d**)).

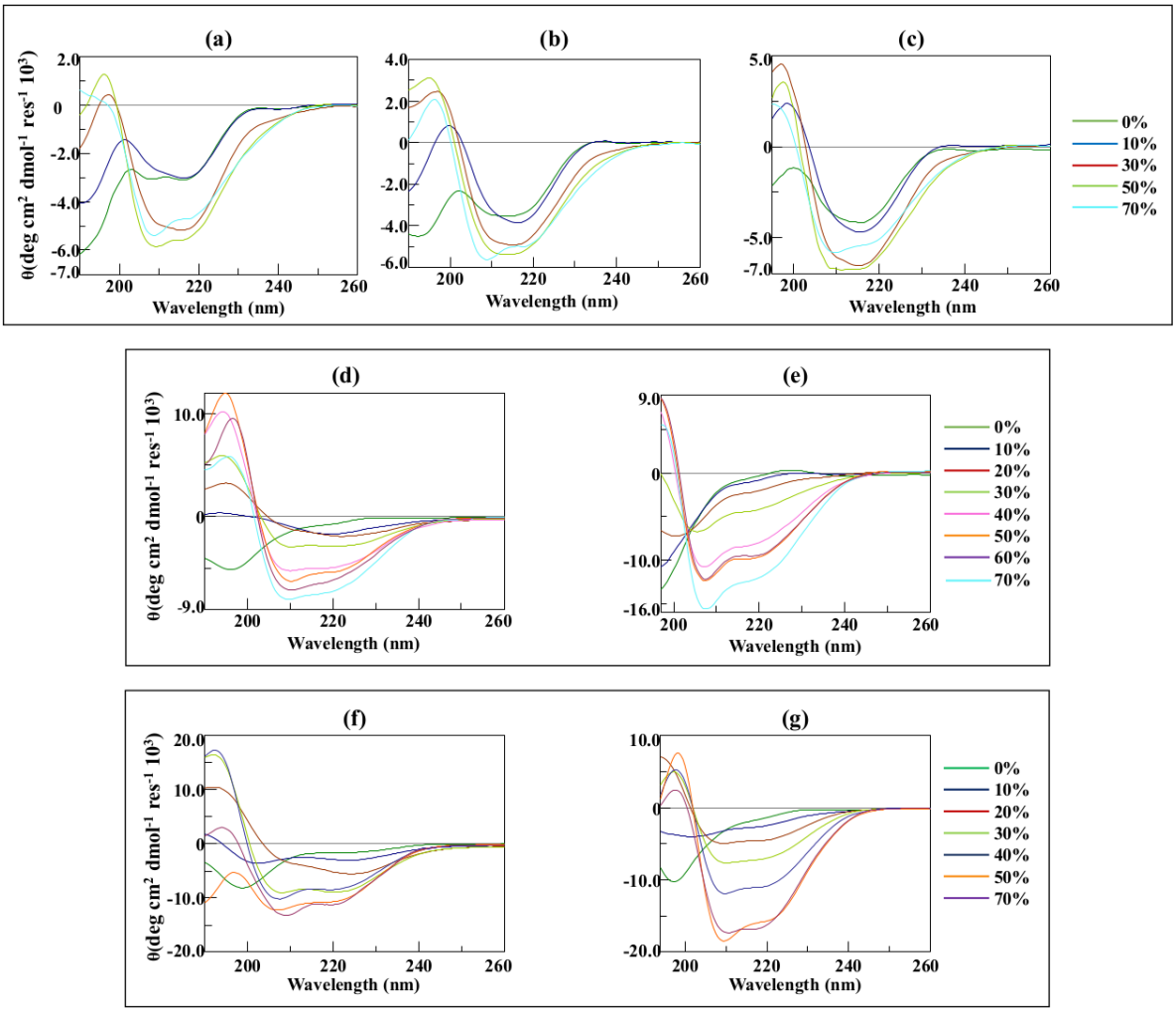

Fig. 2: CD spectra of KRI3 analogues in 10 mM sodium phosphate buffer at increasing amounts of TFE (as indicated in the color legends). (**a**) cKRI3, (**b**) Ac-cKRI3-NH_2, (**c**) cKRI3-NH_2, (**d**) Ac-cKRI3, (**e**) KRI3-IM, (**f**) KRI3-YM, (**g**) KRI4. All spectra were recorded from 190 to 260 nm except for 50 and 70 % of TFE conditions (**c**) and 70% of TFE condition (**e**), when spectra were recorded from 195 to 260 nm and from 197 to 260 nm, respectively.

2.2.2. NMR

The 2D [^{1}H, ^{1}H] NOESY spectrum of KRI4 peptide recorded in PBS does not point out the presence of canonical secondary structure elements but appears rather characteristic of a flexible disordered conformation, for the lack of a conspicuous number of NOE cross-peaks (Supplementary Material - Fig. S11), consequently, a detailed structural study was not achievable. On the contrary, in a solution of PBS/TFE (50/50 v/v), this sequence assumes a more organized structuration as indicated by several rather intense cross peaks within its 2D [^{1}H, ^{1}H] NOESY spectrum (Supplementary Material -Fig. S12). By comparing 2D [^{1}H, ^{1}H] TOCSY and 2D [^{1}H, ^{1}H] NOESY spectra (Supplementary Material

-Fig. S12), an almost complete proton resonance assignment was achieved (Supplementary Material -Table S9) [25]. Comparison of observed Hα chemical shifts values with the random coil ones ($\Delta\delta_{H\alpha}$ values) points out the presence of a helical conformation encompassing the whole peptide sequence (Fig. 3(**a**)) [26]. Indeed, the pattern of NOE contacts is canonical of helical conformations including NOEs of the type Hαi-H_Ni+3; Hαi-Hβi+3; Hαi-H_Ni+4; Hαi-H_Ni+2 (Fig. 3(**b**)). Interestingly, while the contacts Hαi-H_Ni+4 are more representative of the α-helix conformation, those Hαi-H_Ni+2 are indicative of the 3.10 helix [25]. Accordingly, the structure of KRI4 (Fig. 3(**c**); Table S11) presents a somehow distorted helical arrangement encompassing the whole primary sequence. Analysis with the software MOLMOL [27] highlights two α-helical segments covering, in most of the 20 NMR conformers, residues from Ala4 to Ile8 and residues from Ile13 to Ala19, while a more disordered bend/turn arrangement is involving the residues enclosed between these two segments (Fig. 3(**c**)).

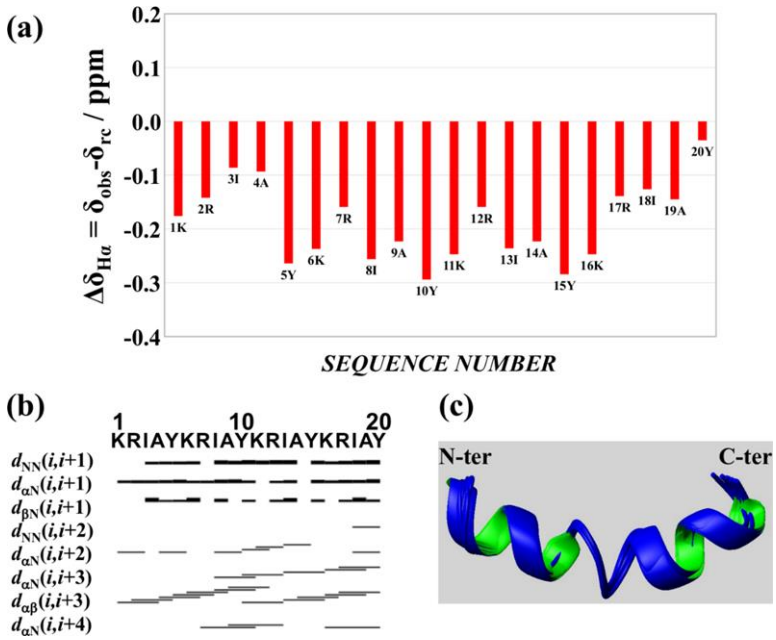

Fig. 3: (**a**) Chemical shift deviations of KRI4 peptide Hα protons from random coil values calculated in PBS/TFE 50/50 v/v. Random coil chemical shifts were evaluated at 298 K and pH 6.9. (**b**) KRI4 peptide NOEs pattern in 50% TFE; "dxy(i, i+1)" stands for a NOE correlation between protons x and y in the i and i+1 residues, respectively; the thickness of each bar is proportional to the corresponding NOE intensity. (**c**) Ribbon representation of KRI4 NMR ensemble of structures obtained in presence of 50% TFE. The final structure calculation includes 324 distance restraints (124 intra-residue, 101 short-, 97 medium- and 2 long-range) along with 104 angle constraints. The best twenty KRI4 NMR conformers, with the lowest target function values, are superimposed on the backbone atoms of residues from 1 to 20 (RMSD in Table S10).

Also for the KRI3-IM peptide NMR studies in PBS buffer (Supplementary Material -Fig. S13) highlights the lack of secondary structure elements, but in PBS/TFE the spectra (Supplementary Material -Fig. S14) indicates a poor dispersion of peaks pointing out a disorder even under strong structuring conditions, in agreement with CD analysis.

Concerning the cyclic KRI3 analogues, a deep investigation was conducted on the cKRI3 peptide for which NMR spectra were recorded in PBS, PBS/TFE 50/50 v/v and in H_2O/TFE 50/50 v/v. In line with results collected for linear peptides, cKRI3 is flexible and disordered in PBS buffer (pH 6.8). However, the process of resonance assignment (Supplementary Material -Table S11) could be completed through comparison of 2D [^{1}H, ^{1}H] NOESY and TOCSY spectra (Supplementary Material -Fig. S15). Chemical shift deviations of Hα protons from random coil values (i.e., $\Delta\delta_{H\alpha}$ (Fig. 4(**a**)) highlights small deviations indicative of a random coil peptide [28, 29] as also indicated by the NOE pattern (Fig. 4(**b**)) that is dominated by sequential Hαi-H_Ni+1 contacts (Fig. 4(**b**) left panel) [25]. In the mixture PBS/TFE 50/50 v/v at pH 7.1 the peptide maintains mainly a disordered character with a majority of negative $\Delta\delta_{H\alpha}$ (Fig. 4(**a**)) that could point to some residual turn/bend structuration although, the NOE pattern is still characteristic of a random coil species (Fig. 4(**b**) middle panel) [25, 28]. In PBS/TFE many H_N peaks are broad and it is rather difficult to get unambiguous proton resonance assignments for a few residues (Supplementary Material -Fig.s S16-S17(**a**) and Table S12); line broadening of H_N residues is likely indicating either high solvent exposure and/or interconversion of different conformers or the presence in solution of small aggregated species. In TFE/H_2O 50/50 v/v solution it is possible to better analyze the conformational preferences of the peptide as higher quality NMR spectra can be recorded and all H_N amide proton resonances can be identified (Supplementary Material -Fig.s S16-S17(**b**) and Table S13). $\Delta\delta_{H\alpha}$ values for the peptide in H_2O/TFE are still mainly small to draw a clear conclusion about the presence of an ordered structural arrangement but, the $\Delta\delta_{H\alpha}$ pattern resembles that of a β-hairpin composed of two β-strands encompassing peptide fragments 4-9 and 12-16 and a bend in between them (Fig. 4(**a**)) [28]. Nevertheless, the NOE pattern is still mainly represented by sequential contacts characteristic of

extended β-structures with only two NOEs of the type Hαi-H_Ni+2 representative of a possible turn/bend (Fig. 4(**b**) right panel) [25]. It is worth noting that CD studies highlight for the peptide a certain β-structuration (Supplementary Material -Table S2).

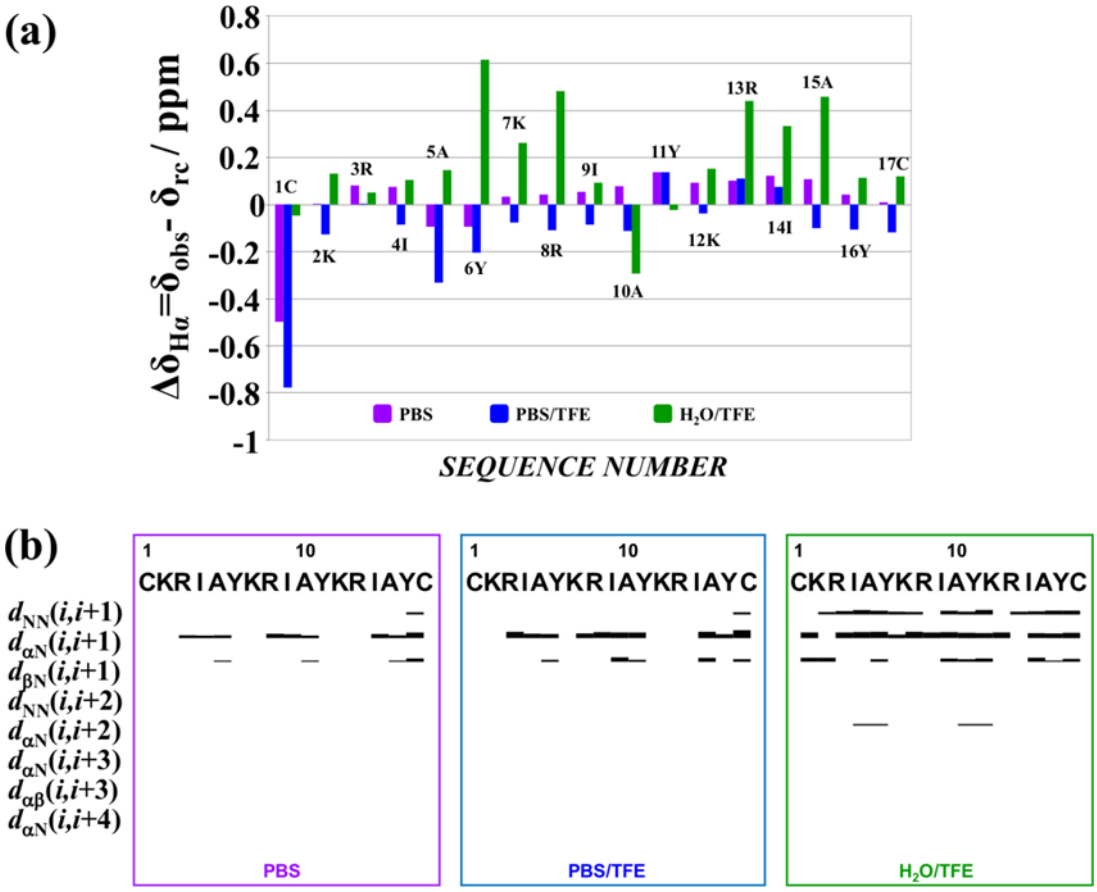

Fig. 4: Conformational analysis of cKRI3 peptide by NMR. (**a**) cKRI3 CSD of Hα atoms with respect to random coil values (=$\Delta\delta_{H\alpha}$) under different experimental conditions (PBS pH 6.8, PBS/TFE pH 7.1, H_2O/TFE pH 2.7, labeled violet, blue and green, respectively). (**b**) cKRI3 NOEs patterns calculated in PBS (inside the violet rectangle) in PBS/TFE (inside the blue rectangle) and in H_2O/TFE (inside the green rectangle).

Structural calculations for the cKRI3 peptide in H_2O/TFE show indeed a flexible cyclic arrangement and a structure that can be described in term of multiple conformational families (Fig. 5). The 20 NMR conformers of the cKRI3 ensemble (Supplementary Material -Table S14) were subjected to a clusterization procedure that generated 5 clusters of conformationally related families: cluster 1 (containing models 1, 2, 3, 5, 7, 8, 12, 14, 15, 18, 19); cluster 2 (including models 4, 9, 13, 16, 20); cluster 3 (including models 6 and 10); clusters 4 and 5 including only 1 model each (number 17 and 11, respectively) [30, 31]. The structures appear characterized only by a reduced number of H-bonds

(Supplementary Material -Table S15) with a rather different pattern among different families of conformers [32].

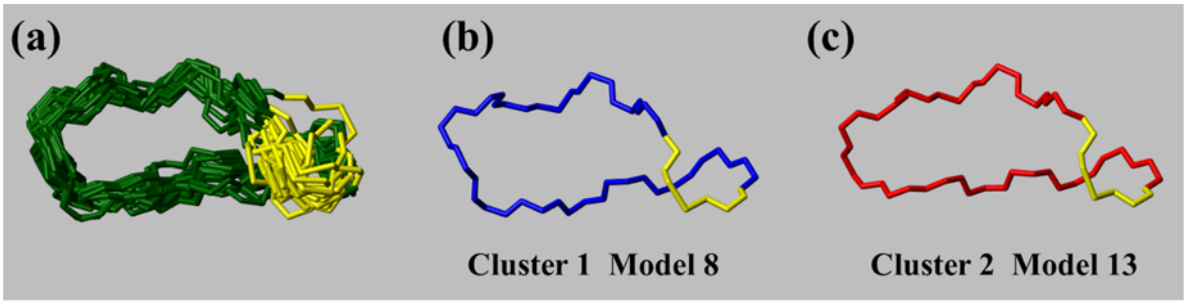

Fig. 5: NMR structure of cKRI3 peptide and cluster analysis. (**a**) The twenty NMR conformers of cKRI3 peptide are superimposed on the backbone atoms and represented in neon. In the final structure calculation 81 angle and 159 distance restraints were implemented. Distance restraints comprised 156 upper distance limits (53 intra-residue, 56 sequential, 20 medium and 27 long-range) and three lower distance restraints necessary to enforce the disulfide bridge. (**b, c**) Representative models of most populated clusters are shown. In each panel peptide conformers are visualized as N, CA, CO backbone trace and with Cys1 and Cys17 backbone and side chains atoms performing a disulfide bridge coloured yellow.

Ac-cKRI3-NH_2 peptide was analyzed in PBS (Supplementary Material -Fig. S18) and PBS/TFE (50/50 v/v) (Supplementary Material -Fig. S19). Proton resonance assignments (Supplementary Material -Tables S16 and S17) could be achieved for many residues by a canonical protocol [25] and also through comparison with chemical shifts observed for the cKRI3 peptide. In PBS H_N proton resonances for Ac-cKRI3-NH_2 result rather broad. The observed line broadening could be linked to solvent-exposure, flexibility (disorder) and conformational exchange, but in part also to the presence in solution of small peptide aggregates. Several H_N peaks remain broad and could not be assigned even in presence of 50% TFE (Supplementary Material -Fig. S19 and Table S17). $\Delta\delta_{H\alpha}$ values point out for Ac-cKRI3-NH_2 a certain amount of β-structuration in the peptide segment Lys7-Cys17 in PBS that slightly increases upon addition of TFE (Supplementary Material -Fig. S20) [33]. These results appear again in agreement with CD data indicating in the peptide the presence of some β-secondary structure (Fig.s 2(**b**) and S4 and Table S3).

NMR spectra were also recorded for Ac-cKRI3 peptide in PBS (Supplementary Material -Fig. S21): they show the prevalence of a disordered state largely lacking canonical secondary structure elements.

2.3. Interaction studies with Ship2-Sam

2.3.1 NMR studies

NMR interaction assays were conducted though [^{1}H, ^{15}N] HSQC spectra that were acquired for ^{15}N labelled Ship2-Sam in absence and presence of peptides [14, 34]. Binding sites on Ship2-Sam were established by looking at the largest chemical shift and peak intensity changes caused by each peptide in the protein spectrum. We initially focused on the linear KRI3 peptide analogues; Fig. S22 reports the NMR interaction assay conducted with the KRI4 peptide. By adding increasing amount of the peptide to the protein, the Ship2-Sam/KRI4 complex tends to precipitate thus largely reducing the quality of NMR experiments and hampering detailed studies of the interaction. Precipitation also accompanies formation of the Ship2-Sam/KRI3 complex [14] but for KRI4, the issue is much more severe and in fact, it was only possible to study the Ship2-Sam/KRI4 interaction using a protein/peptide concentration ratio equal to 1/3 (Supplementary Material -Fig. S22). NMR studies highlight that KRI4 is indeed targeting the ML surface of Ship2-Sam, as residues within this region along with those in the close α5 C-terminal helix (Fig.s 1 and S22), undergo the largest chemical shift and/or intensity changes upon addition of peptide. However, as observed with the KRI3 peptide, NMR data point also out that there is in Ship2-Sam another negatively charged region at the interface of α1-α2 helices (Fig. 1) that at the highest concentrations might be targeted by the peptide (Supplementary Material -Fig. S22(**d,e**)) [14]. As all these charged Ship2-Sam regions become covered by KRI4, the protein/peptide complex precipitates. The phenomenon is indeed a characteristic of other intermolecular interactions that are highly driven by electrostatic contacts and are often affected by a certain unspecific character and aggregation such as protein/DNA complexes [35]. Due to this behavior, it was not possible to quantify the strength of the Ship2-Sam/KRI4 interaction and we conclude that an additional KRIAY motif may favor more unspecific interactions and aggregation with regions outside the ML site.

Next, we investigated binding of KRI3-YM peptide to Ship2-Sam (Supplementary Material -Fig. S23). Only a few very small variations could be revealed in the spectra of the protein recorded in

presence of peptide, thus proving that KRI3-YM is unable to relevantly bind Ship2-Sam. This result is in agreement with docking studies pointing out the importance of the tyrosine residue for the interaction of KRI3 with the ML surface of Ship2-Sam.

As concerning KRI3-IM, NMR data show that the peptide is able to bind Ship2-Sam ML interface (Fig. 6). Intriguingly, the number of protein peaks in the HSQC spectrum that undergo the largest effects in term of chemical shifts and intensity perturbations upon addition of the peptide to the protein (Fig. 6), is lower with respect to what observed for KRI3 peptide (Supplementary Material -Fig. S24) when comparing spectra run at a similar protein/peptide ratio (1 to 24 for KRI3-IM and 1 to 30 for KRI3) and choosing equal thresholds to look for CSP and intensity variations.

Similar experiments were conducted with the cyclic KRI3 analogues (Supplementary Material -Figs. S25-S28). Cyclic peptides behave as Ship2-Sam ligands and produce changes in the HSQC spectra of the protein (Supplementary Material -Fig. S25-S28(**a-c**)). Mapping of changes on the 3D structure of Ship2-Sam indicate that large effects involve residues belonging to the ML Interface and adjacent regions (Supplementary Material -Fig. S25-S28(**d,e**)). However, also for these cyclic peptides unspecific interactions affecting a few protein residues outside the ML interaction area, could be detected (Supplementary Material -Fig. S25-S28(**d,e**)) at the largest peptide/protein concentration ratios used during NMR titration experiments. This effect is particularly severe for the Ac-cKRI3 peptide, in fact, an almost complete disappearance of protein signals occurs by adding the peptide at 300 μM concentration to Ship2-Sam (25 μM concentration). Therefore, the CSP and intensity variations analysis could be achieved only employing a two-fold excess of peptide with respect to the protein (Supplementary Material -Fig. S28). However, even at this low peptide/protein concentration ratio, the interaction with Ac-cKRI3 seems to involve in an unspecific manner most residues along the whole Ship2-Sam sequence (Supplementary Material -Fig. S28(**d, e**)).

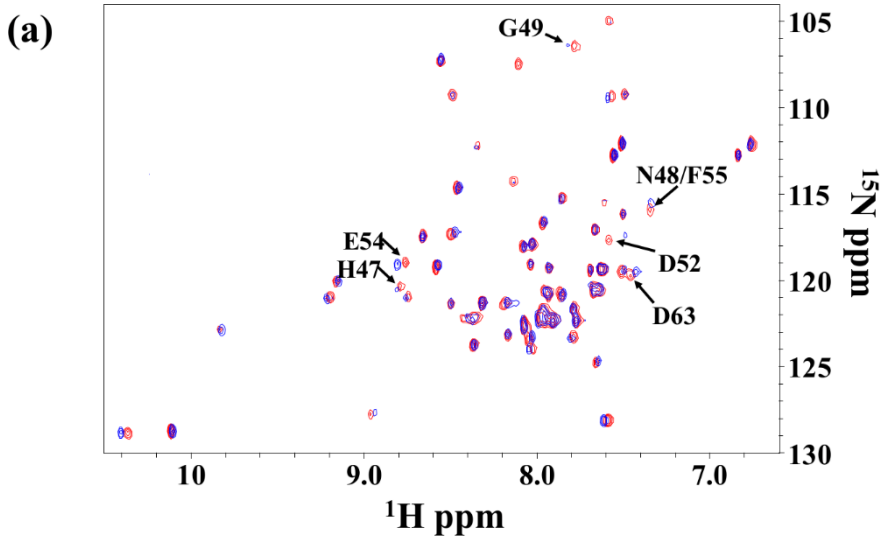
(a)
G49
N48/F55
E54
H47
D52
D63
105
110
115
120
125
130
^{15}N ppm
10
9.0
8.0
7.0
^{1}H ppm

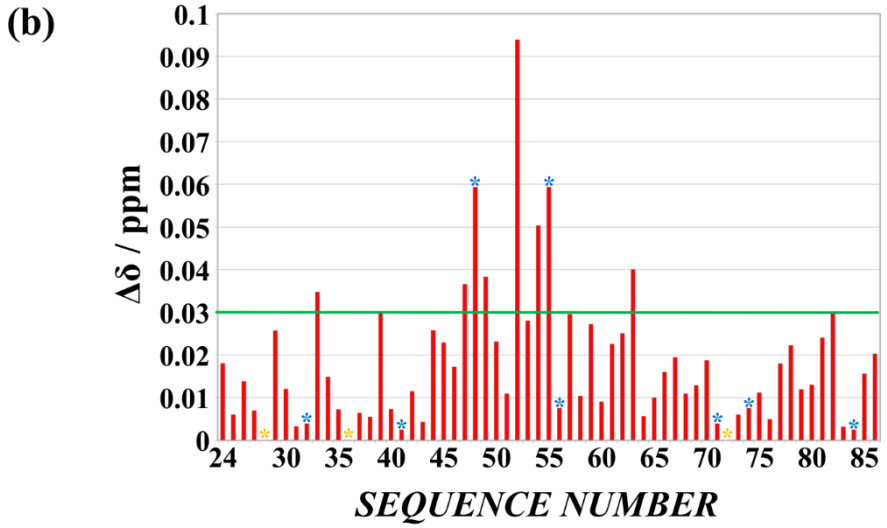
(b)
Δδ / ppm
0.1
0.09
0.08
0.07
0.06
0.05
0.04
0.03
0.02
0.01
0
24 30 35 40 45 50 55 60 65 70 75 80 85
SEQUENCE NUMBER

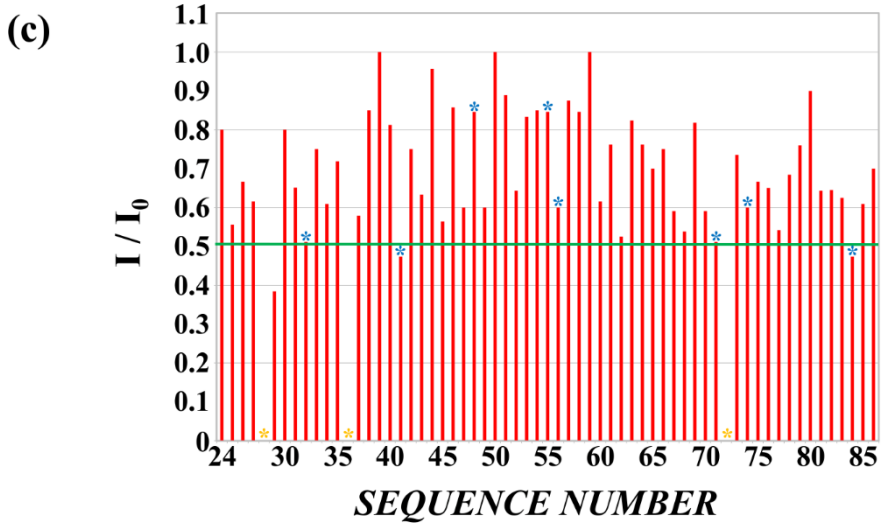
(c)
I / I$_0$
1.1
1.0
0.9
0.8
0.7
0.6
0.5
0.4
0.3
0.2
0.1
0
24 30 35 40 45 50 55 60 65 70 75 80 85
SEQUENCE NUMBER

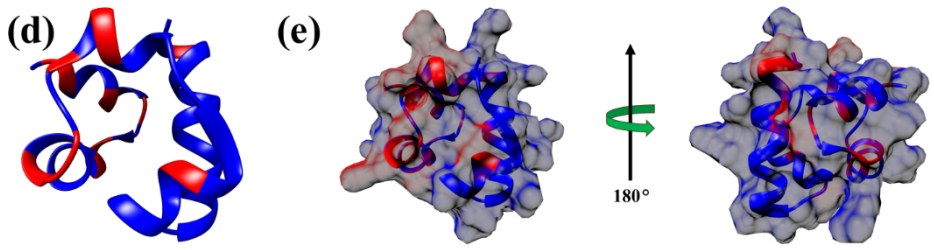
(d)
(e)
180°

Fig. 6: (**a**) Overlay of [^{1}H-^{15}N] HSQC spectra of Ship2-Sam (25 μM concentration) alone (red) and after addition of the KRI3-IM peptide (600 μM concentration) (blue). A few residues with major chemical shift or intensity changes upon addition of the peptide are indicated by black labels. (**b**) Graph of normalized chemical shift deviations (Δδ) as function of residue numbers. (**c**) Graph of I/I_0 (I = intensity of cross-peaks in the HSQC spectrum of the protein in presence of the peptide, I_0 = intensity of H_N cross-peaks in the HSQC spectrum of the protein alone) *versus* residue numbers. Δδ and I/I_0 values are set equal to zero for P72 along with G28 and I36 (orange stars) whose peaks disappear in the spectrum of the peptide/protein complex. The same Δδ and I/I_0 values are attributed ambiguously to the residue pairs W32 and D71, Y41 and L84, N48 and F55, L56 and H74 (blue stars) due to spectral overlaps. (**d, e**) Amino-acids with $\Delta\delta \geq 0.03$ ppm (i.e., L33, E39, H47, N48, G49, D52, E54, F55, D63, L82) and with $I/I_0 \leq 0.5$ (i.e., M29, Y41, L84) are coloured in red on the 3D solution structure of Ship2-Sam (conformer number 1, PDB entry code 2K4P [8]) in its ribbon (**d**) and surfaces (**e**) representations. The residues whose peaks disappear in the spectrum of the peptide/protein complex are coloured in red as well (i.e., G28, I36).

2.3.2. MST and SPR Interaction studies

The interaction between Ship2-Sam and different peptides was further studied by MST technique, but precise measures of dissociation constants (K_D) could not be achieved for the Ac-cKRI3-NH_2, Ac-cKRI3 and cKRI3-NH_2 peptides due to uncanonical shapes of the MST traces by increasing peptide concentrations, that could be possibly linked, in light of NMR experiments, to unspecific interactions (See Supplementary Material -Fig. S29 for Ac-cKRI3-NH_2, Fig. S30 for Ac-cKRI3 and Fig. S31 for cKRI3-NH_2 for further details). For cKRI3 (Supplementary Material -Fig. S32), since unspecific MST signals occurred at higher concentration with respect to other peptides, a rough estimation of the K_D provided a value in the high micromolar range (K_D ~73 ± 5 μM). For KRI3-IM peptide MST traces resulted uncanonical only at concentrations ≥ 800 μM but also in this case the fitting of data indicated a weak binding with a K_D of hundreds of micromolar (K_D ~309 ± 4 μM) (Supplementary Material -Fig. S33).

On the basis of MST results, KRI3-IM and cKRI3 were further investigated by SPR technique. Ship2-Sam was immobilized on the CM5 chip surface and sensorgrams were recorded at increasing peptide amounts. The overlay of sensorgrams related to cKRI3, reported in the Supplementary Material -Fig.

S34 (top panel), clearly indicated a dose-response increase of RU values even if certain unspecific interactions occurred as suggested by uncommon shapes of sensorgrams at high concentrations. The fitting of experimental RU max values vs peptide concentration provided a high micromolar value for dissociation constant, $K_D = (14\pm2)*10^1$ µM (Supplementary Material -Fig. S34) in rather good agreement with MST data. In the case of KRI3-IM, sensorgrams do not follow dose-response profiles, likely due to an unspecific interaction of this sequence with chip matrix. Indeed, starting from 10 µM, lower RU values were observed by increasing peptide concentration (Supplementary Material -Fig. S35).

As interaction assays could be made more challenging by peptide aggregation, Tyr-fluorescence emission spectra were also recorded for cKRI3 and KRI3-IM to evaluate the concentration range, in which structural aggregation does not occur (Fig. S36). Indeed, both the fluorescence intensity and λmax of aromatic residues in proteins/peptides is strictly dependent on the local environment of the fluorophore [36, 37]. In the case of the two peptides the range 100-300 µM provided almost superimposable spectra indicating no significant aggregation, while starting from 500 µM a decrease of fluorescence intensity indicates a quenching effect likely due to the occurrence of aggregation.

Table 2: Summary of interaction data (peptides vs Ship2-Sam).

Peptide	K_D (µM) SPR	K_D (µM) MST
KRI3	83 ± 8[#]	N.D.
KRI3-IM	N.D.	309 ± 4[@]
cKRI3	$(14\pm2)*10^1$	73 ± 5

[#]Value obtained by SPR [14]

[@] The reported value represent the weighted average of two measures

N.D. stands for Not Determined

2.4 Serum stability

To investigate the behavior of linear and cyclic peptides in a cellular context we compared, *in vitro*, the cellular stabilities of cKRI3 and KRI3-IM with respect to KRI3 peptide. To this aim, we followed, during time, the reduction of areas of chromatographic peaks of pure peptides upon the incubation with fetal bovine serum (FBS). In Fig. 7(**a**), the area percentages of peptides *versus* time of analysis

are reported. After 5h, KRI3-IM peptide was the most degraded sequence, since it presented a 30% of starting amount, while cKRI3 and KRI3 provided 79 and 65% values, respectively. At longer times of analysis, 17-19h, KRI3-IM was completely degraded while cKRI3 and KRI3 peptides presented a residual amount of 30% and 3%, respectively. The greater stability exhibited by cKRI3 respect to KRI3 is likely due to the presence of a cycle, while the greater degradability of KRI3-IM to the presence of three additional positively charged residues (9 between R and K) with respect to KRI3 sequences (6 between R and K) that are more sensible to proteases' activity [38, 39].

2.5 Cellular uptake and localization

Preliminary cellular localization assays were conducted in the carcinoma prostate cancer cell line (PC-3) that was chosen since its endogenous levels of EphA2 [40, 41] and Ship2 [42] are elevated. To this purpose, the KRI3, cKRI3 and KRI3-IM peptides were conjugated to a fluorescence probe (fluorescein isothiocyanate (FITC)). Internalization of FITC-peptides was followed by confocal laser scanning microscopy under experimental conditions similar to those implemented for FITC-TAT-KRI3 (i.e., after 4 h incubation and 50 μM peptide concentration) [14]. As reported in Fig. 7(**b**, upper panel), the KRI3 peptide has a mainly cytoplasmatic localization.

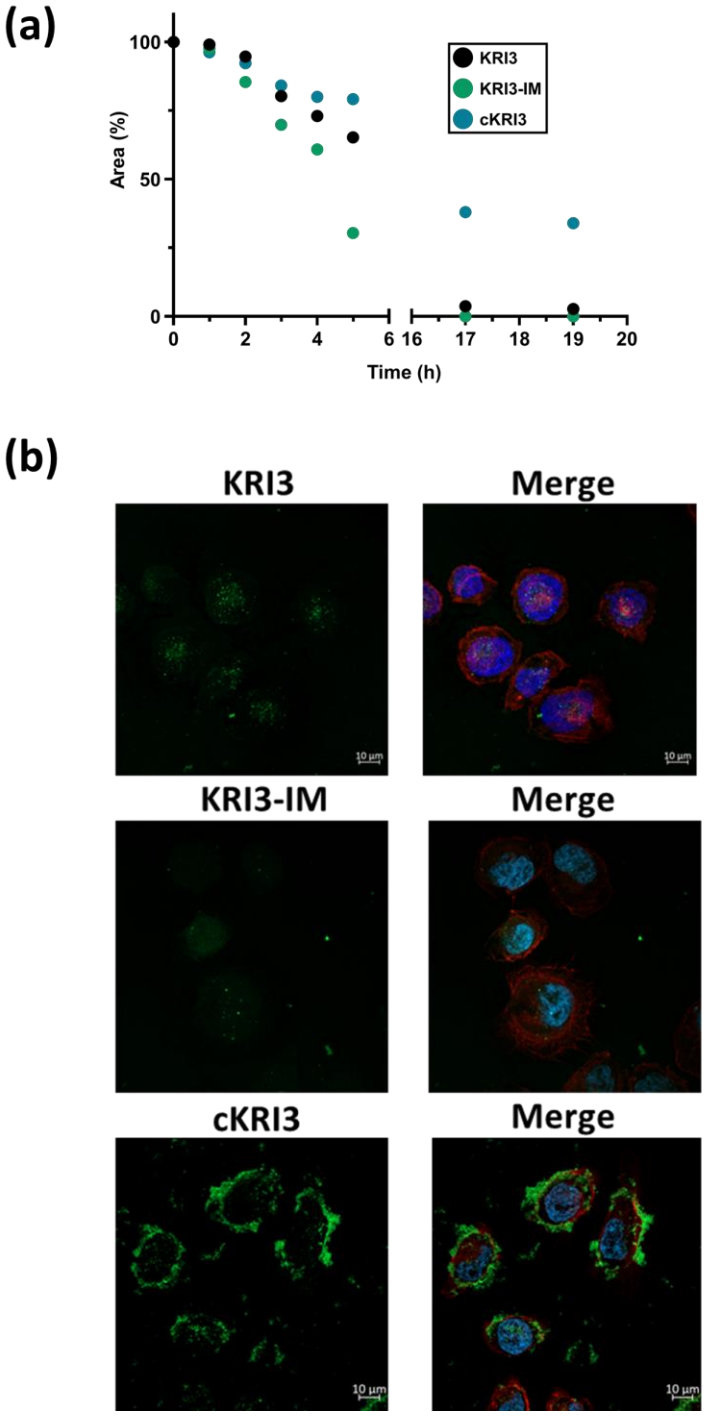

Fig. 7: (**a**) Serum stability assay of indicated peptides, in FBS. (**b**) Confocal laser scanning microscopy of PC-3 cells. Column I corresponds to cells treated with FITC conjugated peptides (50 µM) for 4 hours. Column II corresponds to overlapping of peptides (FITC, green), actin filaments (phalloidin-iFluor 594, red) and nuclei (Hoechst, blue).

Conversely, KRI3-IM and cKRI3 sequences (Fig. 7(**b**) middle and low panels) exhibit different behaviors. FITC-KRI3-IM peptide (Fig. 7(**b**) middle panel) shows poor fluorescent signal, this can be ascribed to the greater proteases' degradation as observed in serum stability assay (Fig. 7(**a**)).

For cKRI3 peptide a diffuse fluorescence signal is observed around the cytoplasmic membrane suggesting the formation of large aggregates whose sizes are not compatible with cellular dimensions thus hampering internalization (Fig. 7(**b**) lower panel) [43].

Conclusion

The heterotypic Sam-Sam interaction between the lipid phosphatase Ship2 and the EphA2 receptor can be considered as a target in anticancer drug-discovery. Targeting the EphA2-Sam/Ship2-Sam interaction is very challenging as Sam-Sam binding interfaces are rather large, flat and dynamic [11]. To date, only very few Sam domain ligands have been described in literature. For instance, more recently DLC1-SAM domain binding peptides with K_{Ds} in the low micromolar range, able to antagonize the interaction with the C2 domain of TNS3 and PTEN and block cancer cell growth and migration by inactivating RhoA, were reported [44]. However, these peptides target the Sam domain of DLC1 that presents a peculiar four helix bundle fold rather different from that of EphA2-Sam and Ship2-Sam [4].

We previously described the "KRI3" peptide that represents a Ship2-Sam ligand working as a weak inhibitor of the EphA2-Sam/Ship2-Sam complex. This new study focuses on the analysis of conformational and interaction preferences of linear and cyclic KRI3 analogues.

A large amount of data was collected through a multidisciplinary approach and indicated that the cyclization of the positively charged KRI3 sequence, through the addition of two cysteine residues at the extremities for the formation of a disulfide bridge, does not increase the affinity towards Ship2-Sam, but, instead, somehow favours aggregation and unspecific interactions despite an improvement of the serum stability of KRI3 consensus sequence.

Structural and interaction studies with the KRI4 peptide point out that addition to the KRI3 sequence of an extra "KRIAY" penta-amino acid motif (Table 1) enhances unspecific effects and protein/peptide complex precipitation in solution, although not changing the overall structural preferences, since in TFE under structuring conditions KRI4 has a tendency to assume helical conformation similarly to KRI3.

In line with results on KRI4, studies with the KRI3-IM peptide, with Ile replaced by Lys (Table 1), stress out that the addition of positive charges is not enough to improve meaningfully the overall specificity and interaction affinity to Ship2-Sam. Furthermore, differently from KRI3, KRI3-IM presents a lower tendency to assume an ordered helical conformation even under strong structuring conditions and presents as well different cellular uptake capacity in PC3.

Moreover, interaction assays with the KRI3-YM linear KRI3 analogue (Table 1), that lacks tyrosine residues, underline the importance of the aromatic residues in the interaction with Ship2-Sam letting speculate that modulating the aromatic character of the KRI3 peptide could be a possible strategy to improve binding to Ship2-Sam. Finally, our preliminary *in vitro* cell-based assays demonstrate the ability of KRI3 to be internalized into PC3 cells even in absence of a cell penetrating peptide sequence.

Based on the results collected herein, to improve binding affinity of KRI3 peptide to Ship2-Sam we can envision to design and investigate novel KRI3 analogues by mutating Tyr to Trp or to unnatural amino-acids like naphthylalanine, the latter should also ensure an improvement of serum stability; in addition, such novel peptides would shed further light on a possible role of the hydroxyl group of Tyrosine in the interaction with Ship2-Sam. Nevertheless, to eventually increase binding specificity and affinity as well as improve stability, we could modulate the conformational properties of KRI3 by generating stapled peptide or scaffold-based cyclic analogues [45]. In order to reduce the unspecific binding connected to electrostatic contacts, it could be interesting to generate KRI3 analogues with one or more positively charged residues replaced by polar amino-acids, the latter

should still be able to provide H-bond interactions thus ensuring good solubility without meaningfully decreasing interaction affinity.

This work sheds further light on the KRI3 peptide features that are needed for specific binding to Ship2-Sam and for its employment in a cellular context and provides useful information that could be exploited in the near future to generate a new series of analogues targeting the ML interface of Ship2-Sam and eventually work as anticancer agents.

Material and Methods

Peptide synthesis

The peptides cKRI3, Ac-cKRI3-NH_2, KRI3-YM and KRI4 were purchased from ProteoGenix (Schiltigheim, France). Sequences cKRI3-NH_2, Ac-cKRI3, KRI3-IM, FITC-KRI3, FITC-KRI3-IM and FITC-cKRI3 were synthetized in our laboratories as briefly described below.

Solid-phase peptide synthesis was performed on a fully automated peptide synthesizer Syro (Multisynthech, Germany). HBTU, Oxyma, Fmoc-amino acid derivatives, rink amide and Wang resins were purchased from Calbiochem-Novabiochem. All other chemicals were obtained from Aldrich and were used without further purification unless otherwise stated. All peptides were synthesized following the Fmoc-tBu procedure [15-17]. The detachment of peptides from resin was achieved at 95% of TFA and crude products were isolated upon precipitation in cold diethyl ether. Disulfide bridge was obtained after one night of stirring in 100 mM carbonate buffer, pH 8.5 under oxidation by air. Crude products were identified through ESI-MS analysis on a Thermo (Milan, Italy) LCQ FLEE. Preparative RP-HPLC was carried out on a Shimadzu LC-8A, equipped with an SPD-M10 AV detector on a C18 column at a flow rate of 20 mL/min. Peptide purity (95%) and identity were confirmed by LC-MS. Purified peptides were lyophilized and stored at -20°C until use.

To evaluate cell entry, peptides were conjugated with the FITC (Fluorescein isothiocyanate) fluorophore that was attached to amine N-terminal group in the case of KRI3 and KRI3-IM and to that of the side chain of a Lys at the N-terminus of cKRI3, all with two β-Ala as spacers.

CD Spectroscopy

A Jasco J-810 spectropolarimeter (JASCO Corp, Milan, Italy) was employed to acquire CD spectra (See references [14, 16, 17] for details). Briefly CD spectra were the results of three scans averaging, the subtraction of blanks and the translation of the signal to mean residue ellipticity (deg × cm^2 × $dmol^{-1}$× res^{-1}). Peptide samples (100 μM concentrations) were analyzed in 0.1 cm path-length quartz cuvette. CD analyses were conducted in 10 mM phosphate buffer at pH 7.2 and in H_2O in presence and absence of TFE (from 0 to 70%) for freshly prepared solutions and after 24 hours.

Fluorescence Spectroscopy

Fluorescence Tyr experiments (λexc: 275nm) for cKRI3 and KRI3-IM were carried out at 25 °C in 50 mM phosphate buffer, at indicated concentrations, using a Jasco FP 8300 spectrofluorometer in a 10 mm path-length cuvette.

NMR Spectroscopy

NMR experiments were recorded at 25 ˚C on a Varian Unity Inova 600 MHz spectrometer equipped with a cold probe with peptide samples made up of 500 μL total volumes.

Conformational studies

NMR spectra of cKRI3 peptide were acquired in a mixture made up of Phosphate Buffer Saline (PBS, 10 mM Na_2HPO_4, 1.8 mM KH_2PO_4, 137 mM NaCl, and 2.7 mM KCl, from Sigma-Aldrich, Milan-Italy)/D_2O (Deuterium Oxide, 98% D, Sigma-Aldrich, Milan-Italy) 90/10 v/v, pH 6.8, peptide concentration 0.5 mM; additional NMR experiments were performed in the mixture H_2O/2,2,2-trifluoroethanol-d3 (TFE-d3, 99.5% isotopic purity, Sigma-Aldrich, Milan-Italy) 50/50 v/v, pH 2.7,

peptide concentration 0.6 mM, and in PBS/TFE-d3 50/50 v/v, pH 7.1, peptide concentration 0.6 mM. For Ac-cKRI3-NH_2 peptide NMR spectra were recorded for the peptide dissolved in PBS/D_2O 90/10 v/v, pH 7.2, and in PBS/TFE-d3 50/50 v/v, pH 7.3, at concentrations equal to 0.5 mM and 1.0 mM, respectively. In addition, NMR experiments were acquired also for Ac-cKRI3 after dissolving the peptide in a mixture made up of PBS/D_2O 90/10 v/v, pH 7.2, peptide concentration 0.5 mM. The NMR spectra of KRI3-IM peptide were recorded in PBS/D_2O 90/10 v/v, pH 7.3, and in PBS/TFE-d3 50/50 v/v, pH 7.4, at peptide concentrations equal to 0.7 mM and 0.5 mM, respectively. The NMR spectra of KRI4 peptide were recorded in PBS/D_2O 90/10 v/v, pH 7.3, and in PBS/TFE 50/50 v/v, pH 6.9, peptide concentrations equal to 0.8 mM and 1.6 mM, respectively. For each sample the 1D [^{1}H] spectrum was recorded along with a set of 2D [^{1}H, ^{1}H] experiments. In details, 2D [^{1}H, ^{1}H] TOCSY (Total Correlation Spectroscopy) [46], NOESY (Nuclear Overhauser Enhancement Spectroscopy) [47] and DQFCOSY (Double Quantum-Filtered Correlated Spectroscopy) [48] spectra were acquired usually with 16-64 scans, 128-256 FIDs in t1, 1024 or 2048 data points in t2. Mixing times for TOCSY and NOESY experiments were 70 and 300 ms, respectively. Water suppression was achieved by *Excitation Sculpting* [49]. The Wüthrich protocol was employed to obtain proton resonance assignments [25]. TSP (Trimethylsilyl-3-propionic acid sodium salt-D4, 99% D, Armar Scientific, Switzerland) was used as internal standard for chemical shifts referencing (methyl protons at 0.0 ppm). Spectra were processed with VNMRJ 1.1D (Varian, Italy) and analyzed with the software NEASY [50] contained in CARA (http://www.nmr.ch/).

Chemical shift deviations from random coil values for Hα protons (CSD) were estimated with the protocol suggested by Kjaergaard and collaborators [26]. Random-coil chemical shift reference values were determined at T=25 ˚C and pH 6.8, pH 7.1 and pH 2.7 for cKRI3 peptide in PBS, PBS/TFE 50/50 v/v, and H_2O/TFE 50/50 v/v, respectively. Random-coil chemical shift reference values were estimated at T=25 ˚C and pH 7.2 or pH 7.3 for Ac-cKRI3-NH_2 peptide in PBS and PBS/TFE 50/50 v/v, respectively. Random-coil chemical shift reference values of KRI4 peptide were

estimated at T=25 ˚C and pH 6.9 in PBS/TFE 50/50 v/v (http://www1.bio.ku.dk/english/research/bms/research/sbinlab/groups/mak/randomcoil/script/).

Interaction studies

Interaction of different peptides with Ship2-Sam or EphA2-Sam was evaluated by chemical shift perturbation experiments through [^{1}H, ^{15}N] HSQC spectra recorded with ^{15}N labeled protein [14, 34]. More in detail, to evaluate the interaction between Ship2-Sam and the cKRI3 peptide, HSQC spectra of the protein (25 μM concentration) were acquired in absence and presence of cKRI3 at different concentrations (i.e., 25 μM, 50 μM, 75 μM, 150 μM, 300 μM, 600 μM, and 783 μM). For the Ac-cKRI3-NH_2, cKRI3-NH_2 and KRI3-IM peptides, NMR chemical shift perturbation studies were conducted by recording [^{1}H, ^{15}N] HSQC spectra of Ship2-Sam (25 μM concentration) alone and upon addition of each peptide (25 μM, 50 μM, 75 μM, 150 μM, 300 μM, 600 μM concentrations). In the case of Ac-cKRI3 peptide, spectra were recorded for ^{15}N labeled Ship2-Sam alone (25 μM concentration) and upon addition of different amounts of peptide (i.e., 25 μM, 50 μM and 300 μM peptide concentrations). Chemical shift perturbation experiments were also performed with ^{15}N labeled Ship2-Sam (38 μM concentration) in absence and in presence of the KRI4 peptide (40 μM, 80 μM and 120 μM concentrations).

Interaction assays were finally carried out for KRI3-YM peptide by recording HSQC spectra of ^{15}N labeled Ship2-Sam (25 μM concentration) without and with peptide (833 μM concentration).

For NMR chemical shift perturbation experiments, different peptide aliquots from concentrated stock solutions were added to the protein samples (^{15}N-labeled Ship2-Sam in PBS buffer at pH ~7.4). The pH of samples was kept constant (~7.4) at each point of titration by eventually adjusting it with a few drops of a concentrated NaOH stock solution.

Structure calculations

The NMR solution structures of cKRI3 and KRI4 peptides in a mixture H_2O/TFE (50/50 v/v) and PBS/TFE (50/50 v/v) respectively, were calculated using CYANA 2.1 [51]. Distance constraints in the form of upper distance limits were obtained from integration of peaks in 2D [^{1}H, ^{1}H] NOESY 300 spectra; angular constraints were generated with the GRIDSEARCH module of CYANA [51].

To keep into account the presence of the disulfide bond in the cKRI3 structure calculations three lower and the upper distance limits were added through the "ssbond" macro of CYANA [51].

Structure calculations initiated from 100 random conformers. The 20 structures, provided with the lowest CYANA target functions and better obeying to the distance and angle constraints, were chosen as representative models of the NMR ensemble and further inspected with the programs MOLMOL [27] and ProcheckNMR [52]. UCSF-Chimera [31] was implemented for the cluster analysis of cKRI3 NMR ensemble; clusters of conformational related structures were generated through a clusterization process after superimposing the backbone atoms (N, CA, CO, O) of all peptide residues in the 20 NMR conformers.

MST

MST experiments were performed with a Monolith NT 115 system (Nano Temper Technologies) equipped with 100% LED and 40% IR-laser power as previously reported [14]. Ship2-Sam was labelled using a His-Tag Labeling Kit RED-tris-NTA (Nano Temper Technologies) and was employed at a concentration equal to 100 nM. To monitor binding of peptides (cKRI3, Ac-cKRI3, cKRI3-NH_2, Ac-cKRI3-NH_2, KRI3-IM) to Ship2-Sam, a 16-steps serial dilution (1:1) was prepared (final concentration range was 0.01 µM - 385 µM for Ac-cKRI3, cKRI3-NH_2 and KRI3-IM; final concentration range was 0.008 µM - 250 µM for cKRI3; final concentration range was 0.015 µM - 500 µM for Ac-cKRI3-NH_2). A further titration was conducted for KRI3-IM with a final concentration range between 0.2 µM and 6.4 mM. Peptide samples, in PBS buffer supplemented with 0.05 % Tween-20, were inserted into premium capillaries and assayed at 25 °C. Normalized

fluorescence values at different peptide concentrations were fitted through the equation $fc = Unbound + \frac{(Bound-Unbound)\times c+c(target)+Kd-\sqrt{(c+c(target)+Kd)^2-4c\times c(target)}}{2c(target)}$ [53] contained in the MO-S002 MO Affinity Analysis program. In the equation the fraction bound at a determined peptide concentration ("c") is indicated with f(c). The term "Unbound" refers either to Fnorm (i.e., the normalized fluorescence signal) in the MST mode or to the raw fluorescence counts (initial fluorescence mode) of the protein target alone. Similarly, the term "Bound" refers instead to the Ship2-Sam/peptide complex. The dissociation constant is represented by "Kd" whereas, the final concentration of the target in the assay is indicated as c(target).

Surface Plasmon Resonance

SPR assays were carried out as previously described [14]. Ship2-Sam domain was immobilized on a CM5 sensor chip by using a solution in acetate buffer (10 mM and pH=5.0, Ship2-Sam concentration= 25 μg/mL). The immobilization level was 2065 RU, a flow-rate of 5 μL/min with an injection time of 7 min was implemented. SPR experiments were conducted in HBS (HEPES (10 mM), NaCl (150 mM), EDTA (3 mM), pH 7.4) running buffer with a flow equal to 20 μL/min, contact time equal to 4.5 min. For cKRI3 concentrations were 3, 10, 30, 50, 70, 100, 200, 500, 700 μM, for KRI3-IM peptide 3, 7, 10, 30, 50, 70, 100 μM.

Reference channel signals were subtracted as blanks by employing BIAevaluation program (version 4.1, GE Healthcare) and GraphPad Prism (version 7.00; GraphPad Software, San Diego, California) was used to fit RUmax values *versus* peptide concentrations by nonlinear regression analysis, by using one site binding equation.

Protein expression

Expression and purification protocols for ^{15}N labelled Ship2-Sam were reported in our previous work [8, 14]. The Sam domain was produced as recombinant protein in *E. coli*; a M9 minimal medium

containing 1 g/L of $^{15}NH_4Cl$ was employed to grow bacteria at 37 ˚C till a cell Optical Density $(OD)_{600\ nm}$ equal to ~ 0.6. Afterward, the induction phase was conducted at 25 ˚C overnight by adding to the medium isopropyl β-D-1-thiogalactopyranoside (IPTG) at 1 mM concentration. Purification of the (His)6-containing protein was achieved through affinity chromatography with an Akta Purifier FPLC System (GE Healthcare, Milano, Italy) and a Nickel column. Pure protein was dialyzed against Phosphate Buffer Saline (PBS, 10 mM Na_2HPO_4, 1.8 mM KH_2PO_4, 137 mM NaCl, and 2.7 mM KCl, from Sigma-Aldrich, Milan-Italy) at pH 7.4.

Docking studies

Models of the Ship2-Sam/KRI3 complex were obtained with the Haddock web-server [21]. During calculations, the first conformers of Ship2-Sam (pdb entry code: 2K4P [8]) and KRI3 [14] NMR ensembles of structures were implemented. Active residues for Ship2-Sam were chosen among the solvent exposed ones (solvent exposure, as calculated by MOLMOL [27], equal at least to 30%) belonging to the ML surface of Ship2-Sam, undergoing major chemical shift and/or intensity changes upon interaction with the peptide. In details, Ship2-Sam residues with CSP $\geq$ 0.04 ppm (H47, G49, W50, D52, E54, I59, D63, L64), and with I/I_0 (I = intensity of H_N peaks in HSQC spectrum of protein in presence of the peptide and I_0 = intensity reference values of protein peaks in HSQC spectrum in absence of peptide) $\leq$ 0.2 (E54, S57, D58) were set as active during docking calculations. As concerning the peptide structure, all residues were provided with a solvent exposure equal to at least 30% and were set as active. The N-terminal tail of Ship2-Sam (residues 22-27) was kept fully flexible during docking calculations [8, 9]. The docking protocol included a rigid body energy minimization during which 1000 structures were calculated, followed by semi-flexible simulated annealing of the best 200 solutions, and by a final refinement in water. The resultant 200 models were subjected directly to a clusterization procedure with a RMSD cut-off value of 5 Å.

Serum stability

25% fetal bovine serum (FBS) was incubated at 37 °C for 15 min. The serum was then spiked with peptides to reach a final peptide concentration of 80 μM. The mixtures were incubated at 37 °C. Aliquots of the incubating mixtures (50 μL) were taken out at different time points (0, 1, 2, 3, 4, 5, 17 and 19 h), quenched with 15% trifluoroacetic acid (TFA) (50 μL) and incubated for 15 min at 2 °C. Samples were subsequently centrifuged for 15 min at 3000 rpm to remove serum proteins and analyzed by reverse phase high performance liquid chromatography (RP-HPLC) on a HPLC LC-4000 series (Jasco) using a C18 column from ThermoFisher (Milan, Italy). Gradient elution was performed at 25°C in a gradient starting with buffer A (water 0.1 % TFA) and applying buffer B (acetonitrile 0.1 % TFA) from 5 to 70 % in 20 min. The areas of peaks were integrated at different times.

Cellular uptake and localization

Human prostate cancer cell lines (PC-3) were cultured in RPMI 1640 medium supplemented with 10% fetal bovine serum (FBS) (GIBCO, USA), 2mM L-glutamine (Lonza, Belgium) at 37°C in 5% CO2 humidified atmosphere.

Cells (5 x 10^4 cells/well) were placed on coverslips inside a Petri dish and peptides FITC-conjugated at final concentration of 50 μM were added to cells for 4 hours. After incubation, cells were rinsed three time in PBS and fixed in 4% paraformaldehyde in PBS for 15 min and then were permeabilized with 0.3% Triton-X 100 in PBS for 30 min. Following blocking with 2% bovine serum albumin for 15 min, the coverslips were stained with phalloidin-iFluor 594 (Abcam, Milan, Italy) diluted 1:1000 for 1 hours. Following additional three washing steps in PBS the nuclei were stained with Hoechst 33342 (ThermoFisher, Milan. Italy), that was diluted 1:2000 and left to act for 15 min in the dark. Finally, the coverslips were mounted onto microscope slides with Mowiol (Sigma, Milan Italy) and allowed to cure for at least 48 h for confocal imaging. Images were obtained using an inverted microscope system LSM 980 ZEISS with a 40X oil immersion objective coupled with a Zen 3.1 software.

Conflict of interest:

The authors report no declarations of interest.

Acknowledgements:

Technical assistance was provided by Leopoldo Zona. The GIDRM ("Gruppo Italiano Discussione Risonanze Magnetiche") is kindly acknowledged for the "Annalaura Segre - Donatella Capitani fellowship" to Marian Vincenzi. Concetta Di Natale is supported by a fellowship from Fondazione Umberto Veronesi and Sara La Manna by AIRC fellowship for Italy. The research leading to these results has received funding from AIRC under IG 2021 - ID. 26121 project – P.I. Marilisa Leone.

Graphical abstract

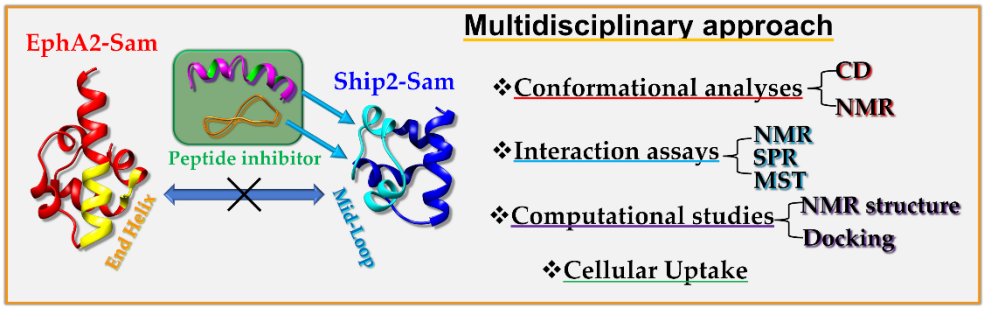

Highlights

- The KRI3 peptide is a previously identified positively charged Ship2-Sam ligand.
- Cyclic and linear KRI3 analogues were evaluated *via* a multidisciplinary approach.
- Tyrosine residues in KRI3 are important for binding to Ship2-Sam.
- Cyclic KRI3 has higher serum stability than KRI3 but worse cellular uptake in PC3.
- KRI3 cellular uptake occurs without conjugation to cell penetrating cargo.

References

[1] M.P. Thomas, C. Erneux, B.V. Potter, SHIP2: Structure, Function and Inhibition, ChemBioChem 18(3) (2017) 233-247.
[2] W. Elong Edimo, S. Schurmans, P.P. Roger, C. Erneux, SHIP2 signaling in normal and pathological situations: Its impact on cell proliferation, Adv. Biol. Regul. 54 (2014) 142-151.
[3] D.F. Lazar, A.R. Saltiel, Lipid phosphatases as drug discovery targets for type 2 diabetes, Nat. Rev. Drug Discov. 5(4) (2006) 333-342.
[4] M. Vincenzi, F.A. Mercurio, M. Leone, Sam Domains in Multiple Diseases, Curr. Med. Chem. 27(3) (2020) 450-476.
[5] G. Zhuang, S. Hunter, Y. Hwang, J. Chen, Regulation of EphA2 receptor endocytosis by SHIP2 lipid phosphatase via phosphatidylinositol 3-Kinase-dependent Rac1 activation, J. Biol. Chem. 282(4) (2007) 2683-2694.
[6] J.H. Raaijmakers, L. Deneubourg, H. Rehmann, J. de Koning, Z. Zhang, S. Krugmann, C. Erneux, J.L. Bos, The PI3K effector Arap3 interacts with the PI(3,4,5)P3 phosphatase SHIP2 in a SAM domain-dependent manner, Cell. Signal. 19(6) (2007) 1249-1257.
[7] H.J. Lee, P.K. Hota, P. Chugha, H. Guo, H. Miao, L.Q. Zhang, S.J. Kim, L. Stetzik, B.C. Wang, M. Buck, NMR Structure of a Heterodimeric SAM:SAM Complex: Characterization and Manipulation of EphA2 Binding Reveal New Cellular Functions of SHIP2, Structure 20(1) (2012) 41-55.
[8] M. Leone, J. Cellitti, M. Pellecchia, NMR studies of a heterotypic Sam-Sam domain association: the interaction between the lipid phosphatase Ship2 and the EphA2 receptor, Biochemistry 47(48) (2008) 12721-12728.

[9] M. Leone, J. Cellitti, M. Pellecchia, The Sam domain of the lipid phosphatase Ship2 adopts a common model to interact with Arap3-Sam and EphA2-Sam, BMC Struct. Biol. 9 (2009) 59.
[10] H. Miao, D.Q. Li, A. Mukherjee, H. Guo, A. Petty, J. Cutter, J.P. Basilion, J. Sedor, J. Wu, D. Danielpour, A.E. Sloan, M.L. Cohen, B. Wang, EphA2 mediates ligand-dependent inhibition and ligand-independent promotion of cell migration and invasion via a reciprocal regulatory loop with Akt, Cancer Cell 16(1) (2009) 9-20.
[11] F.A. Mercurio, M. Leone, The Sam Domain of EphA2 Receptor and its Relevance to Cancer: A Novel Challenge for Drug Discovery?, Curr. Med. Chem. 23(42) (2016) 4718-4734.
[12] F.A. Mercurio, D. Marasco, L. Pirone, E.M. Pedone, M. Pellecchia, M. Leone, Solution structure of the first Sam domain of Odin and binding studies with the EphA2 receptor, Biochemistry 51(10) (2012) 2136-2145.
[13] J. Kim, H. Lee, Y. Kim, S. Yoo, E. Park, S. Park, The SAM domains of Anks family proteins are critically involved in modulating the degradation of EphA receptors, Mol. Cell Biol. 30(7) (2010) 1582-1592.
[14] F.A. Mercurio, C. Di Natale, L. Pirone, R. Iannitti, D. Marasco, E. Pedone, R. Palumbo, M. Leone, The Sam-Sam interaction between Ship2 and the EphA2 receptor: design and analysis of peptide inhibitors, Sci. Rep. 7 (2017) 17474
[15] F.A. Mercurio, C. Di Natale, L. Pirone, D. Marasco, E. Calce, M. Vincenzi, E.M. Pedone, S. De Luca, M. Leone, Design and analysis of EphA2-SAM peptide ligands: A multi-disciplinary screening approach, Bioorg. Chem. 84 (2019) 434-443.
[16] F.A. Mercurio, C. Di Natale, L. Pirone, P.L. Scognamiglio, D. Marasco, E.M. Pedone, M. Saviano, M. Leone, Peptide Fragments of Odin-Sam1: Conformational Analysis and Interaction Studies with EphA2-Sam, ChemBioChem 16(11) (2015) 1629-1636.
[17] F.A. Mercurio, P.L. Scognamiglio, C. Di Natale, D. Marasco, M. Pellecchia, M. Leone, CD and NMR conformational studies of a peptide encompassing the Mid Loop interface of Ship2-Sam, Biopolymers 101(11) (2014) 1088-1098.
[18] F.A. Mercurio, D. Marasco, C. Di Natale, L. Pirone, S. Costantini, E.M. Pedone, M. Leone, Targeting EphA2-Sam and Its Interactome: Design and Evaluation of Helical Peptides Enriched in Charged Residues, ChemBioChem 17(22) (2016) 2179-2188.
[19] F.A. Mercurio, L. Pirone, C. Di Natale, D. Marasco, E.M. Pedone, M. Leone, Sam domain-based stapled peptides: Structural analysis and interaction studies with the Sam domains from the EphA2 receptor and the lipid phosphatase Ship2, Bioorg. Chem. 80 (2018) 602-610.
[20] F.A. Mercurio, C. Di Natale, L. Pirone, M. Vincenzi, D. Marasco, S. De Luca, E.M. Pedone, M. Leone, Exploring the Ability of Cyclic Peptides to Target SAM Domains: A Computational and Experimental Study, ChemBioChem 21(5) (2020) 702-711.
[21] S.J. de Vries, M. van Dijk, A.M. Bonvin, The HADDOCK web server for data-driven biomolecular docking, Nat. Protoc. 5(5) (2010) 883-897.
[22] M. Vincenzi, F.A. Mercurio, M. Leone, About TFE: Old and New Findings, Curr. Protein Pept. Sci. 20(5) (2019) 425-451.
[23] A. Micsonai, F. Wien, L. Kernya, Y.H. Lee, Y. Goto, M. Refregiers, J. Kardos, Accurate secondary structure prediction and fold recognition for circular dichroism spectroscopy, Proc. Natl. Acad. Sci. U. S. A. 112(24) (2015) E3095-103.
[24] A. Jasanoff, A.R. Fersht, Quantitative-Determination of Helical Propensities from Trifluoroethanol Titration Curves, Biochemistry 33(8) (1994) 2129-2135.
[25] K. Wuthrich, NMR of Proteins and Nucleic Acids, Wiley, New YorK, 1986.
[26] M. Kjaergaard, S. Brander, F.M. Poulsen, Random coil chemical shift for intrinsically disordered proteins: effects of temperature and pH, J. Biomol. NMR 49(2) (2011) 139-149.
[27] R. Koradi, M. Billeter, K. Wuthrich, MOLMOL: a program for display and analysis of macromolecular structures, J. Mol. Graph. 14(1) (1996) 51-55.
[28] D.S. Wishart, B.D. Sykes, F.M. Richards, Relationship between nuclear magnetic resonance chemical shift and protein secondary structure, J. Mol. Biol. 222(2) (1991) 311-333.

[29] D.S. Wishart, B.D. Sykes, F.M. Richards, The chemical shift index: a fast and simple method for the assignment of protein secondary structure through NMR spectroscopy, Biochemistry 31(6) (1992) 1647-1651.
[30] L.A. Kelley, S.P. Gardner, M.J. Sutcliffe, An automated approach for clustering an ensemble of NMR-derived protein structures into conformationally related subfamilies, Protein Eng. Des. Sel. 9(11) (1996) 1063-1065.
[31] E.F. Pettersen, T.D. Goddard, C.C. Huang, G.S. Couch, D.M. Greenblatt, E.C. Meng, T.E. Ferrin, UCSF Chimera--a visualization system for exploratory research and analysis, J. Comput. Chem. 25(13) (2004) 1605-1612.
[32] J.E. Mills, P.M. Dean, Three-dimensional hydrogen-bond geometry and probability information from a crystal survey, J. Comput. Aided Mol. Des. 10(6) (1996) 607-622.
[33] D.S. Wishart, B.D. Sykes, F.M. Richards, Simple techniques for the quantification of protein secondary structure by 1H NMR spectroscopy, FEBS Lett. 293(1-2) (1991) 72-80.
[34] M. Pellecchia, B. Becattini, K.J. Crowell, R. Fattorusso, M. Forino, M. Fragai, D. Jung, T. Mustelin, L. Tautz, NMR-based techniques in the hit identification and optimisation processes, Expert Opin. Ther. Targets 8(6) (2004) 597-611.
[35] J. Amato, L. Cerofolini, D. Brancaccio, S. Giuntini, N. Iaccarino, P. Zizza, S. Iachettini, A. Biroccio, E. Novellino, A. Rosato, M. Fragai, C. Luchinat, A. Randazzo, B. Pagano, Insights into telomeric G-quadruplex DNA recognition by HMGB1 protein, Nucleic Acids Res. 47(18) (2019) 9950-9966.
[36] A. Singh, S. Khatun, A. Nath Gupta, Simultaneous Detection of Tyrosine and Structure-Specific Intrinsic Fluorescence in the Fibrillation of Alzheimer's Associated Peptides, Chemphyschem 21(23) (2020) 2585-2598.
[37] D. Florio, C. Di Natale, P.L. Scognamiglio, M. Leone, S. La Manna, S. Di Somma, P.A. Netti, A.M. Malfitano, D. Marasco, Self-assembly of bio-inspired heterochiral peptides, Bioorg. Chem. 114 (2021) 105047.
[38] M. Arias, K.B. Piga, M.E. Hyndman, H.J. Vogel, Improving the Activity of Trp-Rich Antimicrobial Peptides by Arg/Lys Substitutions and Changing the Length of Cationic Residues, Biomolecules 8(2) (2018).
[39] Y.X. Ma, A.F. Yao, X.L. Chen, L. Wang, C.B. Ma, X.P. Xi, T.B. Chen, C. Shaw, M. Zhou, Generation of truncated derivatives through in silico enzymatic digest of peptide GV30 target MRSA both in vitro and in vivo, Comput. Struct. Biotechnol. J. 19 (2021) 4984-4996.
[40] H. Miao, E. Burnett, M. Kinch, E. Simon, B. Wang, Activation of EphA2 kinase suppresses integrin function and causes focal-adhesion-kinase dephosphorylation, Nat. Cell Biol. 2(2) (2000) 62-9.
[41] A. Petty, E. Myshkin, H. Qin, H. Guo, H. Miao, G.P. Tochtrop, J.T. Hsieh, P. Page, L. Liu, D.J. Lindner, C. Acharya, A.D. MacKerell, Jr., E. Ficker, J. Song, B. Wang, A small molecule agonist of EphA2 receptor tyrosine kinase inhibits tumor cell migration in vitro and prostate cancer metastasis in vivo, PLoS One 7(8) (2012) e42120.
[42] R.M. Sharrard, N.J. Maitland, Regulation of protein kinase B activity by PTEN and SHIP2 in human prostate-derived cell lines, Cell. Signal. 19(1) (2007) 129-38.
[43] C. Di Natale, C.F. Natale, D. Florio, P.A. Netti, G. Morelli, M. Ventre, D. Marasco, Effects of surface nanopatterning on internalization and amyloid aggregation of the fragment 264-277 of Nucleophosmin 1, Colloids Surf. B Biointerfaces 197 (2021) 111439.
[44] R. Joshi, L. Qin, X. Cao, S. Zhong, C. Voss, W. Min, S.S.C. Li, DLC1 SAM domain-binding peptides inhibit cancer cell growth and migration by inactivating RhoA, J. Biol. Chem. 295(2) (2020) 645-656.
[45] D. Gang, D.W. Kim, H.S. Park, Cyclic Peptides: Promising Scaffolds for Biopharmaceuticals, Genes (Basel) 9(11) (2018).
[46] C. Griesinger, G. Otting, K. Wuthrich, R.R. Ernst, Clean TOCSY for proton spin system identification in macromolecules, J. Am. Chem. Soc. 110 (1988) 7870-7872.

[47] A. Kumar, R.R. Ernst, K. Wuthrich, A two-dimensional nuclear Overhauser enhancement (2D NOE) experiment for the elucidation of complete proton-proton cross-relaxation networks in biological macromolecules, Biochem. Biophys. Res. Commun. 95(1) (1980) 1-6.
[48] U. Piantini, O.W. Sorensen, R.R. Ernst, Multiple quantum filters for elucidating NMR coupling networks, J. Am. Chem. Soc. 104 (1982) 6800-6801.
[49] T.L. Hwang, A.J. Shaka, Water suppression that works. Excitation sculpting using arbitrary waveforms and pulsed field gradients, J. Magn. Reson. Ser. A 112 (1995) 275-279.
[50] C. Bartels, Xia, T., Billeter, M., Güntert, P. & Wüthrich, K, The program XEASY for computer-supported NMR spectral analysis of biological macromolecules, J. Biomol. NMR 6(1) (1995) 1-10.
[51] T. Herrmann, P. Guntert, K. Wuthrich, Protein NMR structure determination with automated NOE assignment using the new software CANDID and the torsion angle dynamics algorithm DYANA, J. Mol. Biol. 319(1) (2002) 209-227.
[52] R.A. Laskowski, J.A. Rullmannn, M.W. MacArthur, R. Kaptein, J.M. Thornton, AQUA and PROCHECK-NMR: programs for checking the quality of protein structures solved by NMR, J. Biomol. NMR 8(4) (1996) 477-486.
[53] L. Hellinen, S. Bahrpeyma, A.K. Rimpela, M. Hagstrom, M. Reinisalo, A. Urtti, Microscale Thermophoresis as a Screening Tool to Predict Melanin Binding of Drugs, Pharmaceutics 12(6) (2020).

Targeting Ship2-Sam with peptide ligands: novel insights from a multidisciplinary approach

Marian Vincenzi[1@], Flavia Anna Mercurio[1@], Concetta Di Natale[2,3], Rosanna Palumbo[1], Luciano Pirone[1,5], Sara La Manna[4,5], Daniela Marasco[4,5], Emilia Maria Pedone[1,5], and Marilisa Leone[1,5*]

1 Institute of Biostructures and Bioimaging (CNR), Naples, Italy

2 Istituto Italiano di Tecnologia, IIT@CRIB, Naples, Italy

3 Centro di Ricerca Interdipartimentale sui Biomateriali CRIB, University of Naples Federico II, Naples, Italy

4 University of Naples Federico II, Department of Pharmacy, Naples, Italy

5 InterUniversity Research Centre on Bioactive Peptides (CIRPEB), University of Naples Federico II, Naples, Italy

*To whom correspondence should be addressed: Dr. Marilisa Leone. Institute of Biostructures and Bioimaging (CNR), Via Mezzocannone 16, 80134, Naples, Italy. Phone: +39(081) 2534512. Fax: +39(081) 2536642. E-mail: marilisa.leone@cnr.it.

@These authors contributed equally to this work

Keywords: SAM domains, EphA2, Ship2, cancer, NMR, SPR, MST, docking, cellular uptake.

Formatted: Justified

Abstract

The lipid phosphatase Ship2 binds the EphA2 receptor through a heterotypic Sam-Sam (Sterile alpha motif) interaction. Inhibitors of the Ship2-Sam/EphA2-Sam complex hold a certain potential as novel anticancer agents. The previously reported "KRI3" peptide binds Ship2-Sam working as a weak antagonist of the EphA2-Sam/Ship2-Sam interaction. Herein, the design and functional evaluation of KRI3 analogues, both linear and cyclic, are described. A multidisciplinary study was conducted through computational docking techniques, and conformational analyses by CD and NMR spectroscopies. The ability of new peptides to bind Ship2-Sam was analysed by NMR, MST and SPR assays. Studies on linear KRI3 analogues pointed out that aromatic interactions through tyrosines are important for the association with Ship2-Sam whereas, an increase of the net positive charge of the sequence or peptide cyclization through a disulfide bridge can favour unspecific interactions without a substantial improvement of the binding affinity to Ship2-Sam. Interestingly, preliminary cell-based assays demonstrated KRI3 cellular uptake even without the conjugation to a cell penetrating sequence with a main cytosolic localization. This work highlights important features of the KRI3 peptide that can be further exploited to design analogues able to hamper Sam-Sam interactions driven by electrostatic contacts.

1. Introduction

Ship2 (Src homology 2 domain-containing inositol 5'-phosphatase 2) is a lipid phosphatase belonging to the 5'-phosphatases enzyme family [1]. It catalyzes mainly conversion of PIP3 (phosphatidylinositol 3,4,5-triphosphate) in phosphatidylinositol (3,4) P2 and consequently, induces downregulation of different PI3K (Phosphatidyl-Inositol 3 Kinase) activated pathways. Ship2 has several protein interactors and plays roles in physiological and pathological events [2]. For instance it is involved in actin cytoskeletal reorganization, receptor internalization, cell adhesion and spreading [1]. Ship2 regulates insulin sensitivity and obesity and represents a prominent target in drug discovery for type 2 diabetes. In addition, a connection has been established between Ship2 and other diseases

including opsismodysplasia (i.e., a pathology affecting bone development), atherosclerosis, and cancer [1]. The role of Ship2 in cancer is somehow controversial as it can play pro- and anti-tumorigenic functions based on the cell model [2]. Interestingly, Ship2 contains within its modular domain organization a Sam (Sterile alpha motif) domain (Fig. 1) [3]. Sam domains represent small protein binding modules made up of roughly 70 amino acids that fold in a five helix bundle [4]. The Sam domain of Ship2 (Ship2-Sam) is able to associate with the Sam domain of the EphA2-receptor (EphA2-Sam) [5] and the Sam domain of the PI3K effector protein Arap3 (Arap3-Sam) [6]. NMR and molecular modeling studies indicated that Ship2-Sam binds both EphA2-Sam and Arap3-Sam by forming heterodimers with identical interaction topologies [7-9].

Biophysical studies showed low micromolar dissociation constants for these heterotypic Sam-Sam interactions [8, 9]. In detail, Ship2-Sam binds the partner Sam domains through the canonical Mid-Loop (ML)/End Helix (EH) model of Sam-Sam complexes in which Ship2-Sam central region forms the so called ML Interface (Fig. 1) while the EH Interface is provided by part of the C-terminal α5 helices and close α1α2 loops in either EphA2-Sam and Arap3-Sam [7-9].

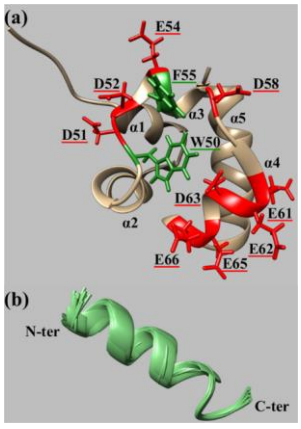

Fig. 1: (**a**) NMR solution structure of Ship2-Sam (pdb code: 2K4P [8], conformer n.1) in a ribbon representation, negatively charged and aromatic residues within the ML Interface are shown in red and green, respectively and labeled with the one letter amino acid codes and sequence numbers. (**b**) NMR solution structure of KRI3 peptide (PBS/TFE 50/50 v/v) in a ribbon representation. Twenty conformers are overlayed on the backbone atoms.

These Sam-Sam interactions are highly driven by electrostatic contacts as the ML Interface in Ship2-Sam is negatively charged whereas, the EH Interfaces in both Arap3-Sam and EphA2-Sam are positively charged; in addition, a few aromatic residues on both surfaces may contribute additional intermolecular contacts (Fig. 1) [7-9]. The functional role and the cellular pathways of the interaction between Ship2-Sam and Arap3-Sam have not been fully clarified whereas, more studies concerning the Ship2-Sam/EphA2-Sam association have been reported [5, 7].

EphA2 is a tyrosine kinase receptor that represents a critical player in cancer where it exhibits a debated role whose outcomes depend by a fine tuning of a ligand-dependent pro-oncogenic and a ligand independent anti-oncogenic route [10]. EphA2 receptor over-expression has been observed in many solid tumors - like ovarian, lung, pancreatic, breast, prostate cancers, and melanoma [11].

In malignant MDA-MB-231 breast cancer cells Ship2 inhibits EphA2 receptor endocytosis and consequently, Ship2 silencing enhances receptor internalization and degradation upon stimulation with an ephrin ligand [5]. To play this function Ship2 needs to be engaged at the receptor through the Ship2-Sam/EphA2-Sam association although also the catalytic activity of Ship2 is required [5].

In our laboratory we have long been focused on the Sam domain of the receptor (EphA2-Sam) to develop inhibitors of its heterotypic interactions with Ship2-Sam and the first Sam domain of the protein Odin (Odin-Sam1) [12]. Ship2 inhibits receptor endocytosis and consequent degradation [5] whereas, Sam domains of the protein Odin are important to enhance receptor stability likely through inhibition of ubiquitination [13]. To achieve our goal, we set up a variety of approaches to design peptide ligands of ML and EH surfaces [14-17]: sequences enriched in charged and helix promoting residues [18], stapled [19] and head to tail cyclic [20] peptides. Interestingly, through a protein dissection approach focused on EphA2-Sam we generated the KRI3 peptide (Table 1) [14]. This sequence, that targets the ML interface of Ship2-Sam, contains the -KRIAY- motif, located into the C-terminal helix in the EH site of EphA2-Sam (aa 956-960 in human EphA2 (Uniprot code P29317)) repeated thrice in tandem [14]. KRI3 was conceived considering that the binding site of Ship2-Sam

for EphA2-Sam is negatively charged and also contains a few aromatic residues (a phenylalanine and a tryptophan) (Fig. 1) and thus, the positive Lys and Arg residues along with the aromatic Tyr could provide several favorable intermolecular contacts [14]. KRI3 interacts with Ship2-Sam with a dissociation constant K_D~100 μM (in SPR (Surface Plasmon Resonance) experiments) and is a weak antagonist of the EphA2-Sam/Ship2-Sam association. NMR (Nuclear Magnetic Resonance) experiments in aqueous solution containing 50% 2,2,2-trifluoroethanol (TFE) provided a structure with an extended helical conformation (Fig. 1(**b**)) [14]. Noticeably, conjugated to Tat-derived cell penetrating peptide (CPP), KRI3 ~~peptide~~ induces necrosis in the PC-3 prostate cancer cell line and is more cytotoxic in cancer cells with respect to normal dermal fibroblasts [14].

With this in mind, starting from the KRI3 sequence, herein we designed and analyzed different linear and cyclic analogues (Table 1).

Table 1: Peptide sequences analyzed in the manuscript. Residues in common with KRI3 sequence are coloured red. Mutated amino acids in KRI3-IM and KRI3-YM are highlighted in blue together with the additional KRIAY motif in KRI4.

Peptide	Sequences
KRI3	Ac-KRIAYKRIAYKRIAY-NH_2
KRI3-YM	Ac-KRIA**A**KRIA**A**KRIA**A**-NH_2
KRI3-IM	Ac-KR**K**AYKR**K**AYKR**K**AY-NH_2
KRI4	Ac-KRIAYKRIAYKRIAY**KRIAY**-NH_2
cKRI3	CKRIAYKRIAYKRIAYC
Ac-cKRI3-NH_2	Ac-CKRIAYKRIAYKRIAYC-NH_2
Ac-cKRI3	Ac-CKRIAYKRIAYKRIAYC
cKRI3-NH_2	CKRIAYKRIAYKRIAYC-NH_2

Ac=N-terminal acetylation, NH_2=C-terminal amidation.

To study this novel peptide series against Ship2-Sam, we performed a multidisciplinary analysis made up of computational and experimental techniques including docking studies, conformational analyses, *in vitro* binding assays through NMR, MST (MicroScale Thermophoresis) and SPR. In addition, we evaluated the cellular localization of KRI3 and a few of its analogues to compare the effects of introduced chemical modifications.

Formatted: Justified

2. Results and Discussion

2.1. Peptide design

Docking studies were conducted with Haddock [21] to get models of the Ship2-Sam/KRI3 complex. The protein docking site was set in the ML surface of Ship2-Sam following analysis of CSP (Chemical Shift Perturbation) data [14] and intensity changes of peaks in the [^{1}H, ^{15}N] spectrum of the protein upon addition of the KRI3 peptide (Supplementary Material - Fig. S1). For such studies the NMR structure of KRI3 calculated in solution containing 50% TFE was implemented [14] (Supplementary Material - Fig. S2). As evaluable from Fig. S2, a helical KRI3 peptide can be well located inside the ML interface of Ship2-Sam establishing multiple contacts (Supplementary Material - Table S1). In detail, the central -KRIAY- motif provides the largest number of interactions; in general, the positive lysines and arginines are responsible for a wide number of intermolecular interactions with the ML interface (1237 and 1345, respectively) along with the tyrosines (number of provided interactions equal to 1369). This is due to the negative and aromatic nature of the ML interface of Ship2-Sam (Fig. 1) [8]. To validate docking results a series of new analogues were designed and their sequences are reported in Table 1. Since Tyr appeared important for the interaction, we designed the KRI3-YM peptide, as negative control, bearing the mutation Tyr/Ala. Instead from docking studies Ile and Ala residues, appeared less involved into the interaction with the protein (providing 909 and 631 intermolecular contacts, respectively), hence, we designed the peptide KRI3-IM where the isoleucines were replaced by lysines to enhance electrostatic interactions. Similarly, the peptide KRI4 was conceived with four "KRIAY" stretches repeated in tandem to evaluate the effects of one additional consensus motif. We also designed cyclic cKRI3 analogues (Table 1) in which two cysteine residues were added at the N- and C-termini of the KRI3 sequence and cyclization was achieved through intramolecular disulfide bond formation. In this context, we focused on cKRI3 compounds bearing or not protections at the N- and C-terminal ends as additional modulating factors of the peptide charge for the interaction with Ship2-Sam (Table 1).

2.2. Conformational analysis

To investigate the conformational properties of designed KRI3 peptide analogues, we conducted structural analyses in solution by means of CD and NMR spectroscopy. 2D [^{1}H, ^{1}H] NMR spectra were recorded in aqueous buffer and in the presence of the structuring co-solvent TFE [22]. Short peptides are often flexible and disordered in a merely aqueous environment but TFE is very useful to unveil the conformational tendencies that could characterize their bioactive conformations [22]. CD studies were as well conducted under similar experimental conditions and during time.

2.2.1. CD investigations

Firstly, CD spectra were recorded in H_2O and aqueous sodium phosphate buffer at pH 7.2, at the indicated concentrations of TFE (Fig. 2 and Supplementary Material -Fig.s S3-S9). The overlays of CD spectra of cKRI3, Ac-cKRI3-NH_2 and cKRI3-NH_2 indicate similar conformational behaviors both in buffer (Fig.s 2(**a-c**), Supplementary Material -Fig.s S3-S5(**b**)) and in water (Supplementary Material -Fig.s S3-S5(**a**)). The deconvolutions of CD spectra ~~was~~ were also performed (Supplementary Material -Tables S2-S4) [23]. In absence of TFE, mixed random-beta conformations can be detected for the presence of a ~~two~~ minimuma ~~centered~~ at ~~~ 195 and~~ 218 nm and a negative band under 200 nm, for cKRI3 (F~~f~~ig.2(**a**)) and Ac-cKRI3-NH_2 (F~~f~~ig.2(**b**)). The addition of TFE leads to a more structured conformation both at 30 and 50% of TFE: in the spectra (Fig.s 2(**a-c**)) we observe~~d~~ a coalescence of initial minima in a broad band centered at 218 nm. As general feature, it ~~was~~is difficult to follow TFE-titration with non-canonical CD profiles. In addition, the absence of an isodichroic wavelength, during TFE titration, indicates the coexistence of different equilibria in solution and not a simple two-state mechanism of transition random coil to helix [24]. Further increase of TFE (70%) induces a major helical content for the clear distinction of two minima at 208 and 218 nm (Fig.s 2(**a-c**)). CD analysis during time (t=0, 24h) does not point out relevant conformational changes (Fig.s 2(**a-c**), Supplementary Material -Fig.s S3-S5(**a** left panel) for t=0; -Fig.s S3-S5(**a** right panel, **b**) for t=24 h). Deconvolution indicates that the contribution of uncanonical

Formatted: Font color: Red
Formatted: Font color: Red
Formatted: Font color: Red
Formatted: Font color: Red
Formatted: Font color: Red
Formatted: Font: Bold, Font color: Red
Formatted: Font color: Red
Formatted: Font color: Red
Formatted: Font color: Red, Subscript
Formatted: Font color: Red
Formatted: Font color: Red, Not Superscript/ Subscript
Formatted: Font color: Red
Formatted: Font: Bold, Font color: Red
Formatted: Font color: Red
Formatted: Font color: Red
Formatted: Font color: Red
Formatted: Font color: Red
Formatted: Font color: Red
Formatted: Font color: Red

secondary structures is always prevalent even if the increase of TFE partially stabilizes β-structures till ~ 30%, then, an enhancement of helical content is also estimated (Supplementary Material -Tables S2-S4). For Ac-cKRI3 sequence, at 0% TFE a major random content is evident, by raising TFE percentages an α-helical content can be also detected (Fig.s 2(**d**) and S6(**a** left panel)) and, similarly to other sequences, no conformational changes were evident after 24h (Supplementary Material -Fig.s S6(**a** right panel, **b**)). An extensive TFE titration suggests that the β content is still prevalent with respect to the helical one even at very high TFE amounts (50%) (Supplementary Material -Table S5). Similarly KRI3-IM at 0% TFE exhibits a typical disordered spectrum with a progressive enhancement of helical content at high percentages of TFE (Fig.s 2(**e**), S7(**b**), Table S6(**c,d**)). In this latter case~~,~~ ~~differently from Ac-cKRI3,~~ TFE titration does not reach saturated ellipticity intensity till 70% (v/v).

Also, KRI3-YM (Fig.s 2(**f**), S8) and KRI4 (Fig.s 2(**g**), S9) at 0% TFE exhibit typical random spectra that tend to assume more helical conformations at increasing amounts of TFE (Supplementary Material -Tables S7-S8). No relevant differences during time can be evidenced for both peptides (Supplementary Material -Table S7-S8).

The analysis of Θ_{min}, that is the Θ value at the relative minimum around the wavelength of 222 nm, vs TFE percentages (Supplementary Material -Fig.~~ure~~ S10), indicates that for almost all sequences the highest value is reached at 50% of TFE (~~Figure~~ Fig.s S10(**a-c**),(**f-g**)) except for KRI3-IM peptide whose plateau is reached at 70 % of TFE (Fig.~~ure~~ S10(**e**)) and Ac-cKRI3 that did not exhibit saturation (Fig.~~ure~~ S10(**d**)). ~~No relevant differences during time can be evidences for both peptides (Supplementary Material -Table S7-S8).~~

Formatted: Font: Not Bold

Formatted: Font: 12 pt

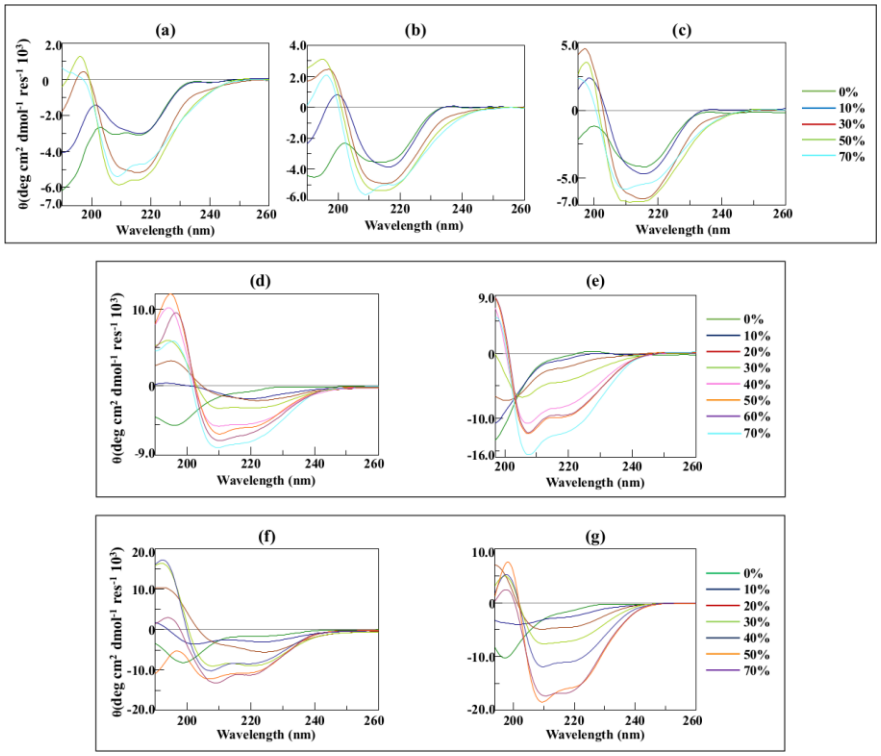

Fig. 2: CD spectra of KRI3 analogues in 10 mM sodium phosphate buffer at increasing amounts of TFE (as indicated in the color legends). (**a**) cKRI3, (**b**) Ac-cKRI3-NH_2, (**c**) cKRI3-NH_2, (**d**) Ac-cKRI3, (**e**) KRI3-IM, (**f**) KRI3-YM, (**g**) KRI4. All spectra were recorded from 190 to 260 nm except for 50 and 70 % of TFE conditions (**c**) and 70% of TFE condition (**e**), when spectra were recorded from 195 to 260 nm and from 197 to 260 nm, respectively.

2.2.2. NMR

The 2D [^{1}H, ^{1}H] NOESY spectrum of KRI4 peptide recorded in PBS does not point out the presence of canonical secondary structure elements but appears rather characteristic of a flexible disordered conformation, for the lack of a conspicuous number of NOE cross-peaks (Supplementary Material - Fig. S1~~0~~), consequently, a detailed structural study was not achievable. On the contrary, in a solution of PBS/TFE (50/50 v/v), this sequence assumes a more organized structuration as indicated by several rather intense cross peaks within its 2D [^{1}H, ^{1}H] NOESY spectrum (Supplementary Material -Fig. S1~~2~~). By comparing 2D [^{1}H, ^{1}H] TOCSY and 2D [^{1}H, ^{1}H] NOESY spectra (Supplementary Material

-Fig. S12~~1~~), an almost complete proton resonance assignment was achieved (Supplementary Material -Table S9) [25]. Comparison of observed Hα chemical shifts values with the random coil ones ($\Delta\delta_{H\alpha}$ values) points out the presence of a helical conformation encompassing the whole peptide sequence (Fig. 3(**a**)) [26]. Indeed, the pattern of NOE contacts is canonical of helical conformations including NOEs of the type Hαi-H_Ni+3; Hαi-H_βi+3; Hαi-H_Ni+4; Hαi-H_Ni+2 (Fig. 3(**b**)). Interestingly, while the contacts Hαi-H_Ni+4 are more representative of the α-helix conformation, those Hαi-H_Ni+2 are indicative of the 3.10 helix [25]. Accordingly, the structure of KRI4 (Fig. 3(**c**); Table S1~~0~~0) presents a somehow distorted helical arrangement encompassing the whole primary sequence. Analysis with the software MOLMOL [27] highlights two α-helical segments covering, in most of the 20 NMR conformers, residues from Ala4 to Ile8 and residues from Ile13 to Ala19, while a more disordered bend/turn arrangement is involving the residues enclosed between these two segments (Fig. 3(**c**)).

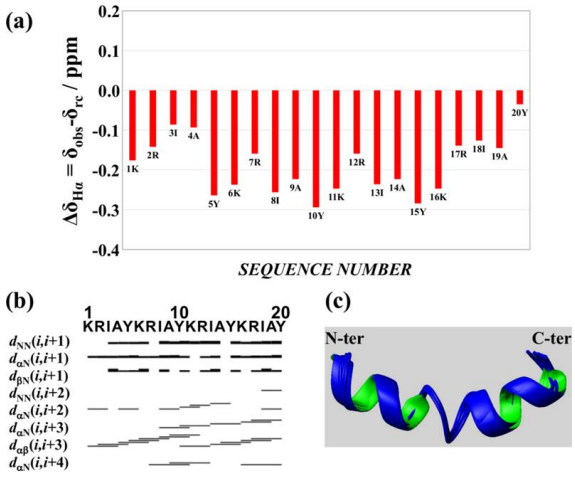

Fig. 3: (**a**) Chemical shift deviations of KRI4 peptide Hα protons from random coil values calculated in PBS/TFE 50/50 v/v. Random coil chemical shifts were evaluated at 298 K and pH 6.9. (**b**) KRI4 peptide NOEs pattern in 50% TFE; "dxy(i, i+1)" stands for a NOE correlation between protons x and y in the i and i+1 residues, respectively; the thickness of each bar is proportional to the corresponding NOE intensity. (**c**) Ribbon representation of KRI4 NMR ensemble of structures obtained in presence of 50% TFE. The final structure calculation includes 324 distance restraints (124 intra-residue, 101 short-, 97 medium- and 2 long-range) along with 104 angle constraints. The best twenty KRI4 NMR

conformers, with the lowest target function values, are superimposed on the backbone atoms of residues from 1 to 20 (RMSD in Table S10).

Also for the KRI3-IM peptide NMR studies in PBS buffer (Supplementary Material -Fig. S132) highlights the lack of secondary structure elements, but in PBS/TFE the spectra (Supplementary Material -Fig. S143) indicates a poor dispersion of peaks pointing out a disorder even under strong structuring conditions, in agreement with CD analysis.

Concerning the cyclic KRI3 analogues, a deep investigation was conducted on the cKRI3 peptide for which NMR spectra were recorded in PBS, PBS/TFE 50/50 v/v and in H_2O/TFE 50/50 v/v. In line with results collected for linear peptides, cKRI3 is flexible and disordered in PBS buffer (pH 6.8). However, the process of resonance assignment (Supplementary Material -Table S114) could be completed through comparison of 2D [^{1}H, ^{1}H] NOESY and TOCSY spectra (Supplementary Material -Fig. S154). Chemical shift deviations of Hα protons from random coil values (i.e., $\Delta\delta_{H\alpha}$ (Fig. 4(**a**)) highlights small deviations indicative of a random coil peptide [28, 29] as also indicated by the NOE pattern (Fig. 4(**b**)) that is dominated by sequential Hαi-H_Ni+1 contacts (Fig. 4(**b**) left panel) [25]. In the mixture PBS/TFE 50/50 v/v at pH 7.1 the peptide maintains mainly a disordered character with a majority of negative $\Delta\delta_{H\alpha}$ (Fig. 4(**a**)) that could point to some residual turn/bend structuration although, the NOE pattern is still characteristic of a random coil species (Fig. 4(**b**) middle panel) [25, 28]. In PBS/TFE many H_N peaks are broad and it is rather difficult to get unambiguous proton resonance assignments for a few residues (Supplementary Material -Fig.s S165-S176(**a**) and Table S12); line broadening of H_N residues is likely indicating either high solvent exposure and/or interconversion of different conformers or the presence in solution of small aggregated species. In TFE/H_2O 50/50 v/v solution it is possible to better analyze the conformational preferences of the peptide as higher quality NMR spectra can be recorded and all H_N amide proton resonances can be identified (Supplementary Material -Fig.s S165-S176(**b**) and Table S13). $\Delta\delta_{H\alpha}$ values for the peptide in H_2O/TFE are still mainly small to draw a clear conclusion about the presence of an ordered structural arrangement but, the $\Delta\delta_{H\alpha}$ pattern resembles that of a β-hairpin composed of two β-strands

encompassing peptide fragments 4-9 and 12-16 and a bend in between them (Fig. 4(**a**)) [28]. Nevertheless, the NOE pattern is still mainly represented by sequential contacts characteristic of extended β-structures with only two NOEs of the type Hαi-H_Ni+2 representative of a possible turn/bend (Fig. 4(**b**) right panel) [25]. It is worth noting that CD studies highlight for the peptide a certain β-structuration (Supplementary Material -Table S2).

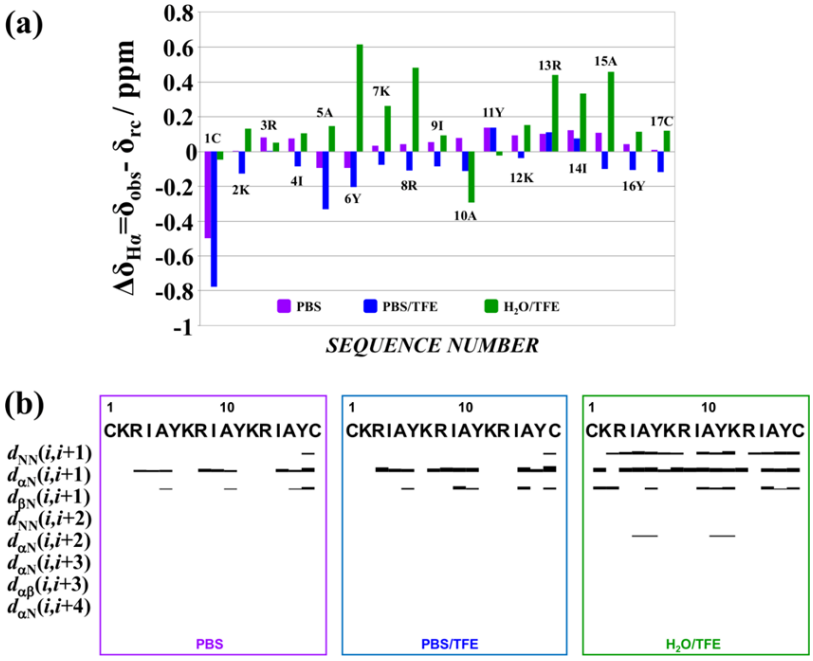

Fig. 4: Conformational analysis of cKRI3 peptide by NMR. (**a**) cKRI3 CSD of Hα atoms with respect to random coil values (=$\Delta\delta_{H\alpha}$) under different experimental conditions (PBS pH 6.8, PBS/TFE pH 7.1, H_2O/TFE pH 2.7, labeled violet, blue and green, respectively). (**b**) cKRI3 NOEs patterns calculated in PBS (inside the violet rectangle) in PBS/TFE (inside the blue rectangle) and in H_2O/TFE (inside the green rectangle).

Structural calculations for the cKRI3 peptide in H_2O/TFE show indeed a flexible cyclic arrangement and a structure that can be described in term of multiple conformational families (Fig. 5). The 20 NMR conformers of the cKRI3 ensemble (Supplementary Material -Table S14) were subjected to a clusterization procedure that generated 5 clusters of conformationally related families: cluster 1 (containing models 1, 2, 3, 5, 7, 8, 12, 14, 15, 18, 19); cluster 2 (including models 4, 9, 13, 16, 20);

cluster 3 (including models 6 and 10); clusters 4 and 5 including only 1 model each (number 17 and 11, respectively) [30, 31]. The structures appear characterized only by a reduced number of H-bonds (Supplementary Material -Table S15) with a rather different pattern among different families of conformers [32].

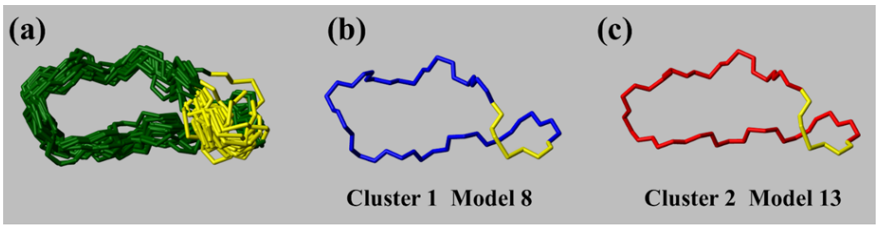

Fig. 5: NMR structure of cKRI3 peptide and cluster analysis. (**a**) The twenty NMR conformers of cKRI3 peptide are superimposed on the backbone atoms and represented in neon. In the final structure calculation 81 angle and 159 distance restraints were implemented. Distance restraints comprised 156 upper distance limits (53 intra-residue, 56 sequential, 20 medium and 27 long-range) and three lower distance restraints necessary to enforce the disulfide bridge. (**b, c**) Representative models of most populated clusters are shown. In each panel peptide conformers are visualized as N, CA, CO backbone trace and with Cys1 and Cys17 backbone and side chains atoms performing a disulfide bridge coloured yellow.

Ac-cKRI3-NH_2 peptide was analyzed in PBS (Supplementary Material -Fig. S187) and PBS/TFE (50/50 v/v) (Supplementary Material -Fig. S198). Proton resonance assignments (Supplementary Material -Tables S16 and S17) could be achieved for many residues by a canonical protocol [25] and also through comparison with chemical shifts observed for the cKRI3 peptide. In PBS H_N proton resonances for Ac-cKRI3-NH_2 result rather broad. The observed line broadening could be linked to solvent-exposure, flexibility (disorder) and conformational exchange, but in part also to the presence in solution of small peptide aggregates. Several H_N peaks remain broad and could not be assigned even in presence of 50% TFE (Supplementary Material -Fig. S198 and Table S17). $\Delta\delta_{H\alpha}$ values point out for Ac-cKRI3-NH_2 a certain amount of β-structuration in the peptide segment Lys7-Cys17 in PBS that slightly increases upon addition of TFE (Supplementary Material -Fig. S2019) [33]. These results appear again in agreement with CD data indicating in the peptide the presence of some β-secondary structure (Fig.s 2(**b**) and S4 and Table S3).

NMR spectra were also recorded for Ac-cKRI3 peptide in PBS (Supplementary Material -Fig. S210): they show the prevalence of a disordered state largely lacking canonical secondary structure elements.

2.3. Interaction studies with Ship2-Sam

2.3.1 NMR studies

NMR interaction assays were conducted though [^{1}H, ^{15}N] HSQC spectra that were acquired for ^{15}N labelled Ship2-Sam in absence and presence of peptides [14, 34]. Binding sites on Ship2-Sam were established by looking at the largest chemical shift and peak intensity changes caused by each peptide in the protein spectrum. We initially focused on the linear KRI3 peptide analogues; Fig. S221 reports the NMR interaction assay conducted with the KRI4 peptide. By adding increasing amount of the peptide to the protein, the Ship2-Sam/KRI4 complex tends to precipitate thus largely reducing the quality of NMR experiments and hampering detailed studies of the interaction. Precipitation also accompanies formation of the Ship2-Sam/KRI3 complex [14] but for KRI4, the issue is much more severe and in fact, it was only possible to study the Ship2-Sam/KRI4 interaction using a protein/peptide concentration ratio equal to 1/3 (Supplementary Material -Fig. S221). NMR studies highlight that KRI4 is indeed targeting the ML surface of Ship2-Sam, as residues within this region along with those in the close α5 C-terminal helix (Fig.s 1 and S221), undergo the largest chemical shift and/or intensity changes upon addition of peptide. However, as observed with the KRI3 peptide, NMR data point also out that there is in Ship2-Sam another negatively charged region at the interface of α1-α2 helices (Fig. 1) that at the highest concentrations might be targeted by the peptide (Supplementary Material -Fig. S221(**d,e**)) [14]. As all these charged Ship2-Sam regions ~~became~~ become covered by KRI4, the protein/peptide complex precipitates. The phenomenon is indeed a characteristic of other intermolecular interactions that are highly driven by electrostatic contacts and are often affected by a certain unspecific character and aggregation such as protein/DNA complexes [35]. Due to this behavior, it was not possible to quantify the strength of the Ship2-Sam/KRI4 interaction and we conclude that an additional KRIAY motif may favor more unspecific interactions and aggregation with regions outside the ML site.

Next, we investigated binding of KRI3-YM peptide to Ship2-Sam (Supplementary Material -Fig. S232). Only a few very small variations could be revealed in the spectra of the protein recorded in presence of peptide, thus proving that KRI3-YM is unable to relevantly bind Ship2-Sam. This result is in agreement with docking studies pointing out the importance of the tyrosine residue for the interaction of KRI3 with the ML surface of Ship2-Sam.

As concerning KRI3-IM, NMR data show that the peptide is able to bind Ship2-Sam ML interface (Fig. 6). Intriguingly, the number of protein peaks in the HSQC spectrum that undergo the largest effects in term of chemical shifts and intensity perturbations upon addition of the peptide to the protein (Fig. 6), is lower with respect to what observed for KRI3 peptide (Supplementary Material -Fig. S243) when comparing spectra run at a similar protein/peptide ratio (1 to 24 for KRI3-IM and 1 to 30 for KRI3) and choosing equal thresholds to look for CSP and intensity variations.

Similar experiments were conducted with the cyclic KRI3 analogues (Supplementary Material -Figs. S254-S287). Cyclic peptides behave as Ship2-Sam ligands and produce changes in the HSQC spectra of the protein (Supplementary Material -Fig. S254-S286(**a-c**)). Mapping of changes on the 3D structure of Ship2-Sam indicate that large effects involve residues belonging to the ML Interface and adjacent regions (Supplementary Material -Fig. S254-S287(**d,e**)). However, also for these cyclic peptides unspecific interactions affecting a few protein residues outside the ML interaction area, could be detected (Supplementary Material -Fig. S254-S287(**d,e**)) at the largest peptide/protein concentration ratios used during NMR titration experiments. This effect is particularly severe for the Ac-cKRI3 peptide, in fact, an almost complete disappearance of protein signals occurs by adding the peptide at 300 μM concentration to Ship2-Sam (25 μM concentration). Therefore, the CSP and intensity variations analysis could be achieved only employing a two-fold excess of peptide with respect to the protein (Supplementary Material -Fig. S287). However, even at this low peptide/protein concentration ratio, the interaction with Ac-cKRI3 seems to involve in an unspecific manner most residues along the whole Ship2-Sam sequence (Supplementary Material -Fig. S287(**d, e**)).

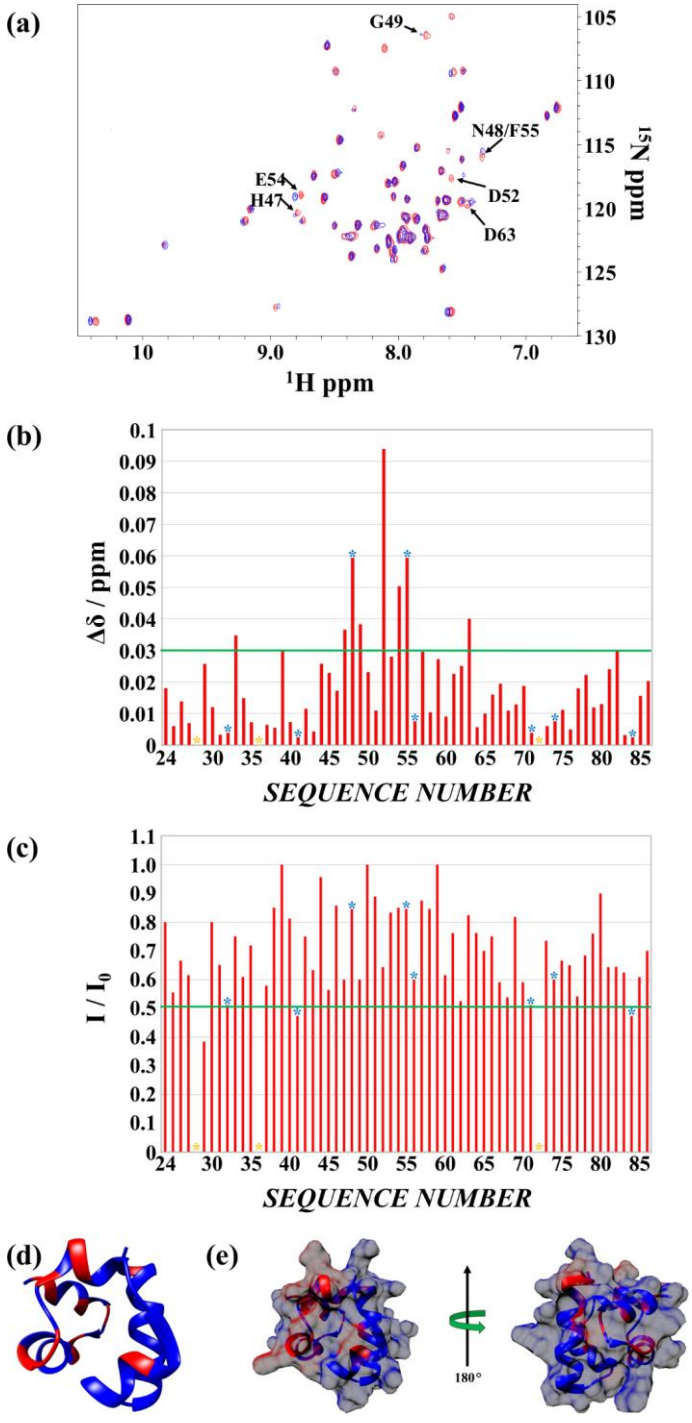
(a)
G49
N48/F55
E54
H47
D52
D63
105
110
115
120
125
130
15N ppm
10
9.0
8.0
7.0
1H ppm
(b)
Δδ / ppm
0.1
0.09
0.08
0.07
0.06
0.05
0.04
0.03
0.02
0.01
0
24 30 35 40 45 50 55 60 65 70 75 80 85
SEQUENCE NUMBER
(c)
I / I0
1.1
1.0
0.9
0.8
0.7
0.6
0.5
0.4
0.3
0.2
0.1
0
24 30 35 40 45 50 55 60 65 70 75 80 85
SEQUENCE NUMBER
(d)
(e)
180°

Fig. 6: (**a**) Overlay of [^{1}H-^{15}N] HSQC spectra of Ship2-Sam (25 µM concentration) alone (red) and after addition of the KRI3-IM peptide (600 µM concentration) (blue). A few residues with major chemical shift or intensity changes upon addition of the peptide are indicated by black labels. (**b**) Graph of normalized chemical shift deviations (Δδ) as function of residue numbers. (**c**) Graph of I/I_0 (I = intensity of cross-peaks in the HSQC spectrum of the protein in presence of the peptide, I_0 = intensity of H_N cross-peaks in the HSQC spectrum of the protein alone) *versus* residue numbers. Δδ and I/I_0 values are set equal to zero for P72 along with G28 and I36 (orange stars) whose peaks disappear in the spectrum of the peptide/protein complex. The same Δδ and I/I_0 values are attributed ambiguously to the residue pairs W32 and D71, Y41 and L84, N48 and F55, L56 and H74 (blue stars) due to spectral overlaps. (**d, e**) Amino-acids with $\Delta\delta \geq 0.03$ ppm (i.e., L33, E39, H47, N48, G49, D52, E54, F55, D63, L82) and with $I/I_0 \leq 0.5$ (i.e., M29, Y41, L84) are coloured in red on the 3D solution structure of Ship2-Sam (conformer number 1, PDB entry code 2K4P [8]) in its ribbon (**d**) and surfaces (**e**) representations. The residues whose peaks disappear in the spectrum of the peptide/protein complex are coloured in red as well (i.e., G28, I36).

2.3.2. MST and SPR Interaction studies

The interaction between Ship2-Sam and different peptides was further studied by MST technique, but precise measures of dissociation constants (K_D) could not be achieved for the Ac-cKRI3-NH_2, Ac-cKRI3 and cKRI3-NH_2 peptides due to uncanonical shapes of the MST traces by increasing peptide concentrations, that could be possibly linked, in light of NMR experiments, to unspecific interactions (See Supplementary Material -Fig. S2~~9~~8 for Ac-cKRI3-NH_2, Fig. S30~~29~~ for Ac-cKRI3 and Fig. S31~~0~~ for cKRI3-NH_2 for further details). For cKRI3 (Supplementary Material -Fig. S32~~1~~), since unspecific MST signals occurred at higher concentration with respect to other peptides, a rough estimation of the K_D provided a value in the high micromolar range (K_D ~73 ± 5 µM). For KRI3-IM peptide MST traces resulted uncanonical only at concentrations ≥ 800 µM but also in this case the fitting of data indicated a weak binding with a K_D of hundreds of micromolar (K_D ~309 ± 4 µM) (Supplementary Material -Fig. S33~~2~~).

On the basis of MST results, KRI3-IM and cKRI3 were further investigated by SPR technique. Ship2-Sam was immobilized on the CM5 chip surface and sensorgrams were recorded at increasing peptide amounts. The overlay of sensorgrams related to cKRI3, reported in the Supplementary Material -Fig.

S343 (top panel), clearly indicated a dose-response increase of RU values even if certain unspecific interactions occurred as suggested by uncommon shapes of sensorgrams at high concentrations. The fitting of experimental RU max values vs peptide concentration provided a high micromolar value for dissociation constant, K_D = (14.0±2)*10^1 µM (Supplementary Material -Fig. S343) in rather good agreement with MST data. In the case of KRI3-IM, sensorgrams do not follow dose-response profiles, likely due to an unspecific interaction of this sequence with chip matrix. Indeed, starting from 10 µM, lower RU values were observed by increasing peptide concentration (Supplementary Material -Fig. S354).

As interaction assays could be made more challenging by peptide aggregation, Tyr-fluorescence emission spectra were also recorded for cKRI3 and KRI3-IM to evaluate the concentration range, in which structural aggregation does not occur (Fig. S36). Indeed, both the fluorescence intensity and λmax of aromatic residues in proteins/peptides is strictly dependent on the local environment of the fluorophore [36, 37]. In the case of the two peptides the range 100-300 µM provided almost superimposable spectra indicating no significant aggregation, while starting from 500 µM a decrease of fluorescence intensity indicates a quenching effect likely due to the occurrence of aggregation.

Table 2: Summary of interaction data (peptides vs Ship2-Sam)

Peptide	K_D (µM) SPR	K_D (µM) MST
KRI3	83 ± 8[#]	N.D.
KRI3-IM	N.D.	309 ± 4[@]
cKRI3	(14.0±2)*10^1	73 ± 5

[#]Value obtained by SPR [14]
[@] The reported value represent the weighted average of two measures
N.D. stands for Not Determined

2.4 Serum stability

To investigate the behavior of linear and cyclic peptides in a cellular context we compared, *in vitro*, the cellular stabilities of cKRI3 and KRI3-IM with respect to KRI3 peptide. To this aim, we followed, during time, the reduction of areas of chromatographic peaks of pure peptides upon the incubation with fetal bovine serum (FBS). In Fig. 7(**a**), the area percentages of peptides *versus* time of analysis

Formatted: Font color: Red
Formatted: Font: Symbol
Formatted: Font: (Default) Times New Roman, 10 pt
Formatted: Justified, Indent: Left: 0", First line: 0.49"
Formatted: Font: (Default) Times New Roman, 10 pt, Bold
Formatted: Font: (Default) Times New Roman, 10 pt
Formatted: Font: (Default) Times New Roman, 10 pt
Formatted: Font: (Default) Times New Roman, 10 pt, Not Italic
Formatted: Font: (Default) Times New Roman, 10 pt, Bold
Formatted: Font: Times New Roman
Formatted: Font: Times New Roman, Subscript
Formatted: Font: Times New Roman
Formatted: Font: Times New Roman
Formatted: Superscript
Formatted: Font: Times New Roman
Formatted: Font: Times New Roman
Formatted: Font: Times New Roman
Formatted Table
Formatted: Superscript
Formatted: Font: Times New Roman
Formatted: Font: Times New Roman
Formatted: Indent: Left: 0", First line: 0.3"

are reported. After 5h, KRI3-IM peptide ~~is~~ was the most degraded sequence, since it presented a 30% of starting amount, while cKRI3 and KRI3 provided 79 and 65% values, respectively. At longer times of analysis, 17-19h, KRI3-IM was completely degraded while cKRI3 and KRI3 peptides presented a residual amount of 30% and 3%, respectively. The greater stability exhibited by cKRI3 respect to KRI3 is likely due to the presence of a cycle, while the greater degradability of KRI3-IM to the presence of three additional positively charged residues (9 between R and K) with respect to KRI3 sequences (6 between R and K) that are more sensible to proteases' activity [38, 39].

2.5 Cellular uptake and localization

Preliminary cellular localization assays were conducted in the carcinoma prostate cancer cell line (PC-3) that was chosen since its endogenous levels of EphA2 [40, 41] and Ship2 [42] are elevated. To this purpose, the KRI3, cKRI3 and KRI3-IM peptides were conjugated to a fluorescence probe (fluorescein isothiocyanate (FITC)). Internalization of FITC-peptides was followed by confocal laser scanning microscopy under experimental conditions similar to those implemented for FITC-TAT-KRI3 (i.e., after 4 h incubation and 50 μM peptide concentration) [14]. As reported in Fig. 7(**b**, upper panel), the KRI3 peptide has a mainly ~~a~~ cytoplasmatic localization.

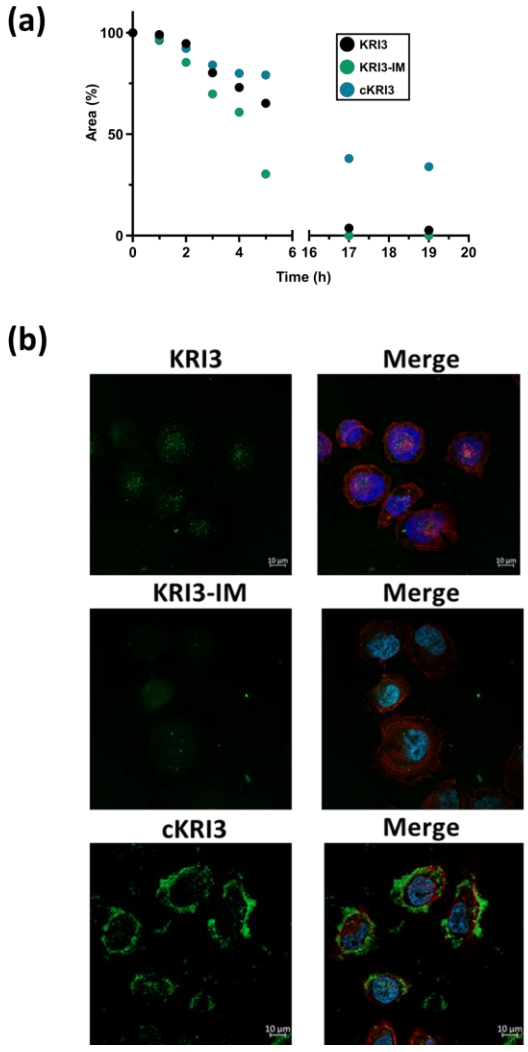

Fig. 7: (**a**) Serum stability assay of indicated peptides, in FBS. (**b**) Confocal laser scanning microscopy of PC-3 cells. Column I corresponds to cells treated with FITC conjugated peptides (50 µM) for 4 hours. Column II corresponds to overlapping of peptides (FITC, green), actin filaments (phalloidin-iFluor 594, red) and nuclei (Hoechst, blue).

Conversely, KRI3-IM and cKRI3 sequences (Fig. 7(**b**) middle and low panels) exhibit different behaviors. FITC-KRI3-IM peptide (Fig. 7(**b**) middle panel) shows poor fluorescent signal, this can be ascribed to the greater proteases' degradation as observed in serum stability assay (Fig. 7(**a**)).

For cKRI3 peptide a diffuse fluorescence signal is observed around the cytoplasmic membrane suggesting the formation of large aggregates whose sizes are not compatible with cellular dimensions thus hampering internalization (Fig. 7(**b**) lower panel) [43].

Conclusion

The heterotypic Sam-Sam interaction between the lipid phosphatase Ship2 and the EphA2 receptor can be considered as a target in anticancer drug-discovery. Targeting the EphA2-Sam/Ship2-Sam interaction is very challenging as Sam-Sam binding interfaces are rather large, flat and dynamic [11]. To date, only very few Sam domain ligands have been described in literature. For instance, more recently DLC1-SAM domain binding peptides with K_{Ds} in the low micromolar range, able to antagonize the interaction with the C2 domain of TNS3 and PTEN and block cancer cell growth and migration by inactivating RhoA, were reported [44]. However, these peptides target the Sam domain of DLC1 that presents a peculiar four helix bundle fold rather different from that of EphA2-Sam and Ship2-Sam [4].

We previously described the "KRI3" peptide that represents a Ship2-Sam ligand working as a weak inhibitor of the EphA2-Sam/Ship2-Sam complex. This new study focuses on the analysis of conformational and interaction preferences of linear and cyclic KRI3 analogues.

A large amount of data was collected through a multidisciplinary approach and indicated that the cyclization of the positively charged KRI3 sequence, through the addition of two cysteine residues at the extremities for the formation of a disulfide bridge, does not increase the affinity towards Ship2-Sam, but, instead, somehow favours aggregation and unspecific interactions despite an improvement of the serum stability of KRI3 consensus sequence.

Structural and interaction studies with the KRI4 peptide point out that addition to the KRI3 sequence of an extra "KRIAY" penta-amino acid motif (Table 1) enhances unspecific effects and protein/peptide complex precipitation in solution, although not changing the overall structural preferences, since in TFE under structuring conditions KRI4 has a tendency to assume helical conformation similarly to KRI3.

In line with results on KRI4, studies with the KRI3-IM peptide, with Ile replaced by Lys (Table 1), stress out that the addition of positive charges is not enough to improve meaningfully the overall specificity and interaction affinity to Ship2-Sam. Furthermore, differently from KRI3, KRI3-IM presents a lower tendency to assume an ordered helical conformation even under strong structuring conditions and presents as well different cellular uptake capacity in PC3.

Moreover, interaction assays with the KRI3-YM linear KRI3 analogue (Table 1), that lacks tyrosine residues, underline the importance of the aromatic residues in the interaction with Ship2-Sam letting speculate that modulating the aromatic character of the KRI3 peptide could be a possible strategy to improve binding to Ship2-Sam. Finally, our preliminary *in vitro* cell-based assays demonstrate the ability of KRI3 to be internalized into PC3 cells even in absence of a cell penetrating peptide sequence.

Based on the results collected herein, to improve binding affinity of KRI3 peptide to Ship2-Sam we can envision to design and investigate novel KRI3 analogues by mutating Tyr to Trp or to unnatural amino-acids like naphthylalanine, the latter should also ensure an improvement of serum stability; in addition, such novel peptides would shed further light on a possible role of the hydroxyl group of Tyrosine in the interaction with Ship2-Sam. Nevertheless, to eventually increase binding specificity and affinity as well as improve stability, we could modulate the conformational properties of KRI3 by generating stapled peptide or scaffold-based cyclic analogues [45]. In order to reduce the unspecific binding connected to electrostatic contacts, it could be interesting to generate KRI3 analogues with one or more positively charged residues replaced by polar amino-acids, the latter

should still be able to provide H-bond interactions thus ensuring good solubility without meaningfully decreasing interaction affinity.

~~Finally, our preliminary *in vitro* cell-based assays demonstrate the ability of KRI3 to be internalized into PC3 cells even in absence of a cell-penetrating peptide sequence.~~

This work sheds further light on the KRI3 peptide features that are needed for specific binding to Ship2-Sam and for its employment in a cellular context and provides useful information that could be exploited in the near future to generate a new series of ~~linear~~ analogues targeting the ML interface of Ship2-Sam and eventually work as anticancer agents.

Material and Methods

Peptide synthesis

The peptides cKRI3, Ac-cKRI3-NH_2, KRI3-YM and KRI4 were purchased from ProteoGenix (Schiltigheim, France). Sequences cKRI3-NH_2, Ac-cKRI3, KRI3-IM, FITC-KRI3, FITC-KRI3-IM and FITC-cKRI3 were synthetized in our laboratories as briefly described below.

Solid-phase peptide synthesis was performed on a fully automated peptide synthesizer Syro (Multisynthech, Germany). HBTU, Oxyma, Fmoc-amino acid derivatives, rink amide and Wang resins were purchased from Calbiochem-Novabiochem. All other chemicals were obtained from Aldrich and were used without further purification unless otherwise stated. All peptides were synthesized following the Fmoc-tBu procedure [15-17]. The detachment of peptides from resin was achieved at 95% of TFA and crude products were isolated upon precipitation in cold diethyl ether. Disulfide bridge was obtained after one night of stirring in 100 mM carbonate buffer, pH 8.5 under oxidation by air. Crude products were identified through ESI-MS analysis on a Thermo (Milan, Italy) LCQ FLEE. Preparative RP-HPLC was carried out on a Shimadzu LC-8A, equipped with an SPD-M10 AV detector on a C18 column at a flow rate of 20 mL/min. Peptide purity (95%) and identity were confirmed by LC-MS. Purified peptides were lyophilized and stored at -20°C until use.

To evaluate cell entry, peptides were conjugated with the FITC (Fluorescein isothiocyanate) fluorophore that was attached to amine N-terminal group in the case of KRI3 and KRI3-IM and to that of the side chain of a Lys at the N-terminus of cKRI3, all with two β-Ala as spacers.

CD Spectroscopy

A Jasco J-810 spectropolarimeter (JASCO Corp, Milan, Italy) was employed to acquire CD spectra (See references [14, 16, 17] for details). Briefly CD spectra were the results of three scans averaging, the subtraction of blanks and the translation of the signal to mean residue ellipticity (deg × cm^2 × $dmol^{-1}$× res^{-1}). Peptide samples (100 μM concentrations) were analyzed in 0.1 cm path-length quartz cuvette. CD analyses were conducted in 10 mM phosphate buffer at pH 7.2 and in H_2O in presence and absence of TFE (from 0 to 70%) for freshly prepared solutions and after 24 hours.

Fluorescence Spectroscopy

Fluorescence Tyr experiments (λexc: 275nm) for cKRI3 and KRI3-IM were carried out at 25 °C in 50 mM phosphate buffer, at indicated concentrations, using a Jasco FP 8300 spectrofluorometer in a 10 mm path-length cuvette.

Formatted: Font: Not Bold

NMR Spectroscopy

NMR experiments were recorded at 25 ˚C on a Varian Unity Inova 600 MHz spectrometer equipped with a cold probe with peptide samples made up of 500 μL total volumes.

Conformational studies

NMR spectra of cKRI3 peptide were acquired in a mixture made up of Phosphate Buffer Saline (PBS, 10 mM Na_2HPO_4, 1.8 mM KH_2PO_4, 137 mM NaCl, and 2.7 mM KCl, from Sigma-Aldrich, Milan-Italy)/D_2O (Deuterium Oxide, 98% D, Sigma-Aldrich, Milan-Italy) 90/10 v/v, pH 6.8, peptide concentration 0.5 mM; additional NMR experiments were performed in the mixture H_2O/2,2,2-trifluoroethanol-d3 (TFE-d3, 99.5% isotopic purity, Sigma-Aldrich, Milan-Italy) 50/50 v/v, pH 2.7,

peptide concentration 0.6 mM, and in PBS/TFE-d3 50/50 v/v, pH 7.1, peptide concentration 0.6 mM. For Ac-cKRI3-NH_2 peptide NMR spectra were recorded for the peptide dissolved in PBS/D_2O 90/10 v/v, pH 7.2, and in PBS/TFE-d3 50/50 v/v, pH 7.3, at concentrations equal to 0.5 mM and 1.0 mM, respectively. In addition, NMR experiments were acquired also for Ac-cKRI3 after dissolving the peptide in a mixture made up of PBS/D_2O 90/10 v/v, pH 7.2, peptide concentration 0.5 mM. The NMR spectra of KRI3-IM peptide were recorded in PBS/D_2O 90/10 v/v, pH 7.3, and in PBS/TFE-d3 50/50 v/v, pH 7.4, at peptide concentrations equal to 0.7 mM and 0.5 mM, respectively. The NMR spectra of KRI4 peptide were recorded in PBS/D_2O 90/10 v/v, pH 7.3, and in PBS/TFE 50/50 v/v, pH 6.9, peptide concentrations equal to 0.8 mM and 1.6 mM, respectively. For each sample the 1D [^{1}H] spectrum was recorded along with a set of 2D [^{1}H, ^{1}H] experiments. In details, 2D [^{1}H, ^{1}H] TOCSY (Total Correlation Spectroscopy) [46], NOESY (Nuclear Overhauser Enhancement Spectroscopy) [47] and DQFCOSY (Double Quantum-Filtered Correlated Spectroscopy) [48] spectra were acquired usually with 16-64 scans, 128-256 FIDs in t1, 1024 or 2048 data points in t2. Mixing times for TOCSY and NOESY experiments were 70 and 300 ms, respectively. Water suppression was achieved by *Excitation Sculpting* [49]. The Wüthrich protocol was employed to obtain proton resonance assignments [25]. TSP (Trimethylsilyl-3-propionic acid sodium salt-D4, 99% D, Armar Scientific, Switzerland) was used as internal standard for chemical shifts referencing (methyl protons at 0.0 ppm). Spectra were processed with VNMRJ 1.1D (Varian, Italy) and analyzed with the software NEASY [50] contained in CARA (http://www.nmr.ch/).

Field Code Changed

Chemical shift deviations from random coil values for Hα protons (CSD) were estimated with the protocol suggested by Kjaergaard and collaborators [26]. Random-coil chemical shift reference values were determined at T=25 ˚C and pH 6.8, pH 7.1 and pH 2.7 for cKRI3 peptide in PBS, PBS/TFE 50/50 v/v, and H_2O/TFE 50/50 v/v, respectively. Random-coil chemical shift reference values were estimated at T=25 ˚C and pH 7.2 or pH 7.3 for Ac-cKRI3-NH_2 peptide in PBS and PBS/TFE 50/50 v/v, respectively. Random-coil chemical shift reference values of KRI4 peptide were

estimated at T=25 ˚C and pH 6.9 in PBS/TFE 50/50 v/v (http://www1.bio.ku.dk/english/research/bms/research/sbinlab/groups/mak/randomcoil/script/).

Field Code Changed

Interaction studies

Interaction of different peptides with Ship2-Sam or EphA2-Sam was evaluated by chemical shift perturbation experiments through [^{1}H, ^{15}N] HSQC spectra recorded with ^{15}N labeled protein [14, 34]. More in detail, to evaluate the interaction between Ship2-Sam and the cKRI3 peptide, HSQC spectra of the protein (25 µM concentration) were acquired in absence and presence of cKRI3 at different concentrations (i.e., 25 µM, 50 µM, 75 µM, 150 µM, 300 µM, 600 µM, and 783 µM). For the Ac-cKRI3-NH_2, cKRI3-NH_2 and KRI3-IM peptides, NMR chemical shift perturbation studies were conducted by recording [^{1}H, ^{15}N] HSQC spectra of Ship2-Sam (25 µM concentration) alone and upon addition of each peptide (25 µM, 50 µM, 75 µM, 150 µM, 300 µM, 600 µM concentrations). In the case of Ac-cKRI3 peptide, spectra were recorded for ^{15}N labeled Ship2-Sam alone (25 µM concentration) and upon addition of different amounts of peptide (i.e., 25 µM, 50 µM and 300 µM peptide concentrations). Chemical shift perturbation experiments were also performed with ^{15}N labeled Ship2-Sam (38 µM concentration) in absence and in presence of the KRI4 peptide (40 µM, 80 µM and 120 µM concentrations).

Interaction assays were finally carried out for KRI3-YM peptide by recording HSQC spectra of ^{15}N labeled Ship2-Sam (25 µM concentration) without and with peptide (833 µM concentration).

For NMR chemical shift perturbation experiments, different peptide aliquots from concentrated stock solutions were added to the protein samples (^{15}N-labeled Ship2-Sam in PBS buffer at pH ~7.4). The pH of samples was kept constant (~7.4) at each point of titration by eventually adjusting it with a few drops of a concentrated NaOH stock solution.

Structure calculations

The NMR solution structures of cKRI3 and KRI4 peptides in a mixture H_2O/TFE (50/50 v/v) and PBS/TFE (50/50 v/v) respectively, were calculated using CYANA 2.1 [51]. Distance constraints in the form of upper distance limits were obtained from integration of peaks in 2D [^{1}H, ^{1}H] NOESY 300 spectra; angular constraints were generated with the GRIDSEARCH module of CYANA [51].

To keep into account the presence of the disulfide bond in the cKRI3 structure calculations three lower and the upper distance limits were added through the "ssbond" macro of CYANA [51].

Structure calculations initiated from 100 random conformers. The 20 structures, provided with the lowest CYANA target functions and better obeying to the distance and angle constraints, were chosen as representative models of the NMR ensemble and further inspected with the programs MOLMOL [27] and ProcheckNMR [52]. UCSF-Chimera [31] was implemented for the cluster analysis of cKRI3 NMR ensemble; clusters of conformational related structures were generated through a clusterization process after superimposing the backbone atoms (N, CA, CO, O) of all peptide residues in the 20 NMR conformers.

Field Code Changed
Formatted: Italian (Italy)
Field Code Changed

MST

MST experiments were performed with a Monolith NT 115 system (Nano Temper Technologies) equipped with 100% LED and 40% IR-laser power as previously reported [14]. Ship2-Sam was labelled using a His-Tag Labeling Kit RED-tris-NTA (Nano Temper Technologies) and was employed at a concentration equal to 100 nM. To monitor binding of peptides (cKRI3, Ac-cKRI3, cKRI3-NH_2, Ac-cKRI3-NH_2, KRI3-IM) to Ship2-Sam, a 16-steps serial dilution (1:1) was prepared (final concentration range was 0.01 µM - 385 µM for Ac-cKRI3, cKRI3-NH_2 and KRI3-IM; final concentration range was 0.008 µM - 250 µM for cKRI3; final concentration range was 0.015 µM - 500 µM for Ac-cKRI3-NH_2). A further titration was conducted for KRI3-IM with a final concentration range between 0.2 µM and 6.4 mM. Peptide samples, in PBS buffer supplemented with 0.05 % Tween-20, were inserted into premium capillaries and assayed at 25 °C. Normalized

fluorescence values at different peptide concentrations were fitted through ~~an~~ the equation $fc = Unbound + \frac{(Bound-Unbound)\times c+c(target)+Kd-\sqrt{(c+c(target)+Kd)^2-4c\times c(target)}}{2c(target)}$ [53] contained in the MO-S002 MO Affinity Analysis program. In the equation the fraction bound at a determined peptide concentration ("c") is indicated with f(c). The term "Unbound" refers either to Fnorm (i.e., the normalized fluorescence signal) in the MST mode or to the raw fluorescence counts (initial fluorescence mode) of the protein target alone. Similarly, the term "Bound" refers instead to the Ship2-Sam/peptide complex. The dissociation constant is represented by "Kd", whereas, the final concentration of the target in the assay is indicated as c(target).

Surface Plasmon Resonance

SPR assays were carried out as previously described [14]. Ship2-Sam domain was immobilized on a CM5 sensor chip by using a solution in acetate buffer (10 mM and pH=5.0, Ship2-Sam concentration= 25 µg/mL). The immobilization level was 2065 RU, a flow-rate of 5 µL/min with an injection time of 7 min was implemented. SPR experiments were conducted in HBS (HEPES (10 mM), NaCl (150 mM), EDTA (3 mM), pH 7.4) running buffer with a flow equal to 20 µL/min, contact time equal to 4.5 min. For cKRI3 concentrations were 3, 10, 30, 50, 70, 100, 200, 500, 700 µM, for KRI3-IM peptide 3, 7, 10, 30, 50, 70, 100 µM.

Reference channel signals were subtracted as blanks by employing BIAevaluation program (version 4.1, GE Healthcare) and Graph-Pad Prism (version 7.00; GraphPad Software, San Diego, California) was used to fit RUmax values *versus* peptide concentrations by nonlinear regression analysis, by using one site binding equation.

Protein expression

Expression and purification protocols for ^{15}N labelled Ship2-Sam were reported in our previous work [8, 14]. The Sam domain was produced as recombinant protein in *E. coli*; a M9 minimal medium

Formatted: English (United States)
Formatted: English (United States)
Formatted: English (United States)
Formatted: English (United States)
Formatted: English (United States)
Formatted: English (United States)
Formatted: English (United States)
Formatted: English (United States)
Formatted: English (United States)
Formatted: English (United States)
Formatted: English (United States)
Formatted: English (United States)
Formatted: English (United States)
Formatted: English (United States)
Formatted: English (United States)
Formatted: Font color: Red

containing 1 g/L of $^{15}NH_4Cl$ was employed to grow bacteria at 37 ˚C till a cell Optical Density $(OD)_{600\ nm}$ equal to ~ 0.6. Afterward, the induction phase was conducted at 25 ˚C overnight by adding to the medium isopropyl β-D-1-thiogalactopyranoside (IPTG) at 1 mM concentration. Purification of the (His)6-containing protein was achieved through affinity chromatography with an Akta Purifier FPLC System (GE Healthcare, Milano, Italy) and a Nickel column. Pure protein was dialyzed against Phosphate Buffer Saline (PBS, 10 mM Na_2HPO_4, 1.8 mM KH_2PO_4, 137 mM NaCl, and 2.7 mM KCl, from Sigma-Aldrich, Milan-Italy) at pH 7.4.

Docking studies

Models of the Ship2-Sam/KRI3 complex were obtained with the Haddock web-server [21]. During calculations, the first conformers of Ship2-Sam (pdb entry code: 2K4P [8]) and KRI3 [14] NMR ensembles of structures were implemented. Active residues for Ship2-Sam were chosen among the solvent exposed ones (solvent exposure, as calculated by MOLMOL [27], equal at least to 30%) belonging to the ML surface of Ship2-Sam, undergoing major chemical shift and/or intensity changes upon interaction with the peptide. In details, Ship2-Sam residues with CSP $\geq$ 0.04 ppm (H47, G49, W50, D52, E54, I59, D63, L64), and with I/I_0 (I = intensity of H_N peaks in HSQC spectrum of protein in presence of the peptide and I_0 = intensity reference values of protein peaks in HSQC spectrum in absence of peptide) $\leq$ 0.2 (E54, S57, D58) were set as active during docking calculations. As concerning the peptide structure, all residues were provided with a solvent exposure equal to at least 30% and were set as active. The N-terminal tail of Ship2-Sam (residues 22-27) was kept fully flexible during docking calculations [8, 9]. The docking protocol included a rigid body energy minimization during which 1000 structures were calculated, followed by semi-flexible simulated annealing of the best 200 solutions, and by a final refinement in water. The resultant 200 models were subjected directly to a clusterization procedure with a RMSD cut-off value of 5 Å.

Serum stability

25% fetal bovine serum (FBS) was incubated at 37 °C for 15 min. The serum was then spiked with peptides to reach a final peptide concentration of 80 µM. The mixtures were incubated at 37 °C. Aliquots of the incubating mixtures (50 µL) were taken out at different time points (0, 1, 2, 3, 4, 5, 17 and 19 h), quenched with 15% trifluoroacetic acid (TFA) (50 µL) and incubated for 15 min at 2 °C. Samples were subsequently centrifuged for 15 min at 3000 rpm to remove serum proteins and analyzed by reverse phase high performance liquid chromatography (RP-HPLC) on a HPLC LC-4000 series (Jasco) using a C18 column from ThermoFisher (Milan, Italy). Gradient elution was performed at 25°C in a gradient starting with buffer A (water 0.1 % TFA) and applying buffer B (acetonitrile 0.1 % TFA) from 5 to 70 % in 20 min. The areas of peaks were integrated at different times.

Cellular uptake and localization

Human prostate cancer cell lines (PC-3) were cultured in RPMI 1640 medium supplemented with 10% fetal bovine serum (FBS) (GIBCO, USA), 2mM L-glutamine (Lonza, Belgium) at 37°C in 5% CO2 humidified atmosphere.

Cells (5 x 10^4 cells/well) were placed on coverslips inside a Petri dish and peptides FITC-conjugated at final concentration of 50 µM were added to cells for 4 hours. After incubation, cells were rinsed three time in PBS and fixed in 4% paraformaldehyde in PBS for 15 min and then were permeabilized with 0.3% Triton-X 100 in PBS for 30 min. Following blocking with 2% bovine serum albumin for 15 min, the coverslips were stained with phalloidin-iFluor 594 (Abcam, Milan, Italy) diluted 1:1000 for 1 hours. Following additional three washing steps in PBS the nuclei were stained with Hoechst 33342 (ThermoFisher, Milan. Italy), that was diluted 1:2000 and left to act for 15 min in the dark. Finally, the coverslips were mounted onto microscope slides with Mowiol (Sigma, Milan Italy) and allowed to cure for at least 48 h for confocal imaging. Images were obtained using an inverted microscope system LSM 980 ZEISS with a 40X oil immersion objective coupled with a Zen 3.1 software.

Formatted: Superscript

Conflict of interest:

The authors report no declarations of interest.

Acknowledgements:

Technical assistance was provided by Leopoldo Zona. The GIDRM ("Gruppo Italiano Discussione Risonanze Magnetiche") is kindly acknowledged for the "Annalaura Segre - Donatella Capitani fellowship" to Marian Vincenzi. ~~and~~ Concetta Di Natale ~~were~~ is supported by a fellowship from Fondazione Umberto Veronesi and~~.~~ Sara La Manna ~~was supported~~ by AIRC fellowship for Italy. The research leading to these results has received funding from AIRC under IG 2021 - ID. 26121 project – P.I. Marilisa Leone.

Graphical abstract

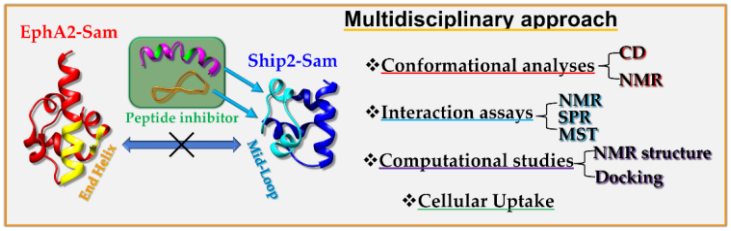

Highlights

- The KRI3 peptide is a previously identified positively charged Ship2-Sam ligand.
- Cyclic and linear KRI3 analogues were evaluated *via* a multidisciplinary approach.
- Tyrosine residues in KRI3 are important for binding to Ship2-Sam.
- Cyclic KRI3 has higher serum stability than KRI3 but worse cellular uptake in PC3.
- KRI3 cellular uptake occurs without conjugation to cell penetrating cargo.

References

[1] M.P. Thomas, C. Erneux, B.V. Potter, SHIP2: Structure, Function and Inhibition, ChemBioChem 18(3) (2017) 233-247.
[2] W. Elong Edimo, S. Schurmans, P.P. Roger, C. Erneux, SHIP2 signaling in normal and pathological situations: Its impact on cell proliferation, Adv. Biol. Regul. 54 (2014) 142-151.
[3] D.F. Lazar, A.R. Saltiel, Lipid phosphatases as drug discovery targets for type 2 diabetes, Nat. Rev. Drug Discov. 5(4) (2006) 333-342.
[4] M. Vincenzi, F.A. Mercurio, M. Leone, Sam Domains in Multiple Diseases, Curr. Med. Chem. 27(3) (2020) 450-476.
[5] G. Zhuang, S. Hunter, Y. Hwang, J. Chen, Regulation of EphA2 receptor endocytosis by SHIP2 lipid phosphatase via phosphatidylinositol 3-Kinase-dependent Rac1 activation, J. Biol. Chem. 282(4) (2007) 2683-2694.
[6] J.H. Raaijmakers, L. Deneubourg, H. Rehmann, J. de Koning, Z. Zhang, S. Krugmann, C. Erneux, J.L. Bos, The PI3K effector Arap3 interacts with the PI(3,4,5)P3 phosphatase SHIP2 in a SAM domain-dependent manner, Cell. Signal. 19(6) (2007) 1249-1257.
[7] H.J. Lee, P.K. Hota, P. Chugha, H. Guo, H. Miao, L.Q. Zhang, S.J. Kim, L. Stetzik, B.C. Wang, M. Buck, NMR Structure of a Heterodimeric SAM:SAM Complex: Characterization and Manipulation of EphA2 Binding Reveal New Cellular Functions of SHIP2, Structure 20(1) (2012) 41-55.

Formatted: Justified
Formatted: English (United States)
Formatted: English (United States)
Formatted: Font: 12 pt

[8] M. Leone, J. Cellitti, M. Pellecchia, NMR studies of a heterotypic Sam-Sam domain association: the interaction between the lipid phosphatase Ship2 and the EphA2 receptor, Biochemistry 47(48) (2008) 12721-12728.
[9] M. Leone, J. Cellitti, M. Pellecchia, The Sam domain of the lipid phosphatase Ship2 adopts a common model to interact with Arap3-Sam and EphA2-Sam, BMC Struct. Biol. 9 (2009) 59.
[10] H. Miao, D.Q. Li, A. Mukherjee, H. Guo, A. Petty, J. Cutter, J.P. Basilion, J. Sedor, J. Wu, D. Danielpour, A.E. Sloan, M.L. Cohen, B. Wang, EphA2 mediates ligand-dependent inhibition and ligand-independent promotion of cell migration and invasion via a reciprocal regulatory loop with Akt, Cancer Cell 16(1) (2009) 9-20.
[11] F.A. Mercurio, M. Leone, The Sam Domain of EphA2 Receptor and its Relevance to Cancer: A Novel Challenge for Drug Discovery?, Curr. Med. Chem. 23(42) (2016) 4718-4734.
[12] F.A. Mercurio, D. Marasco, L. Pirone, E.M. Pedone, M. Pellecchia, M. Leone, Solution structure of the first Sam domain of Odin and binding studies with the EphA2 receptor, Biochemistry 51(10) (2012) 2136-2145.
[13] J. Kim, H. Lee, Y. Kim, S. Yoo, E. Park, S. Park, The SAM domains of Anks family proteins are critically involved in modulating the degradation of EphA receptors, Mol. Cell Biol. 30(7) (2010) 1582-1592.
[14] F.A. Mercurio, C. Di Natale, L. Pirone, R. Iannitti, D. Marasco, E. Pedone, R. Palumbo, M. Leone, The Sam-Sam interaction between Ship2 and the EphA2 receptor: design and analysis of peptide inhibitors, Sci. Rep. 7 (2017) 17474
[15] F.A. Mercurio, C. Di Natale, L. Pirone, D. Marasco, E. Calce, M. Vincenzi, E.M. Pedone, S. De Luca, M. Leone, Design and analysis of EphA2-SAM peptide ligands: A multi-disciplinary screening approach, Bioorg. Chem. 84 (2019) 434-443.
[16] F.A. Mercurio, C. Di Natale, L. Pirone, P.L. Scognamiglio, D. Marasco, E.M. Pedone, M. Saviano, M. Leone, Peptide Fragments of Odin-Sam1: Conformational Analysis and Interaction Studies with EphA2-Sam, ChemBioChem 16(11) (2015) 1629-1636.
[17] F.A. Mercurio, P.L. Scognamiglio, C. Di Natale, D. Marasco, M. Pellecchia, M. Leone, CD and NMR conformational studies of a peptide encompassing the Mid Loop interface of Ship2-Sam, Biopolymers 101(11) (2014) 1088-1098.
[18] F.A. Mercurio, D. Marasco, C. Di Natale, L. Pirone, S. Costantini, E.M. Pedone, M. Leone, Targeting EphA2-Sam and Its Interactome: Design and Evaluation of Helical Peptides Enriched in Charged Residues, ChemBioChem 17(22) (2016) 2179-2188.
[19] F.A. Mercurio, L. Pirone, C. Di Natale, D. Marasco, E.M. Pedone, M. Leone, Sam domain-based stapled peptides: Structural analysis and interaction studies with the Sam domains from the EphA2 receptor and the lipid phosphatase Ship2, Bioorg. Chem. 80 (2018) 602-610.
[20] F.A. Mercurio, C. Di Natale, L. Pirone, M. Vincenzi, D. Marasco, S. De Luca, E.M. Pedone, M. Leone, Exploring the Ability of Cyclic Peptides to Target SAM Domains: A Computational and Experimental Study, ChemBioChem 21(5) (2020) 702-711.
[21] S.J. de Vries, M. van Dijk, A.M. Bonvin, The HADDOCK web server for data-driven biomolecular docking, Nat. Protoc. 5(5) (2010) 883-897.
[22] M. Vincenzi, F.A. Mercurio, M. Leone, About TFE: Old and New Findings, Curr. Protein Pept. Sci. 20(5) (2019) 425-451.
[23] A. Micsonai, F. Wien, L. Kernya, Y.H. Lee, Y. Goto, M. Refregiers, J. Kardos, Accurate secondary structure prediction and fold recognition for circular dichroism spectroscopy, Proc. Natl. Acad. Sci. U. S. A. 112(24) (2015) E3095-103.
[24] A. Jasanoff, A.R. Fersht, Quantitative-Determination of Helical Propensities from Trifluoroethanol Titration Curves, Biochemistry 33(8) (1994) 2129-2135.
[25] K. Wuthrich, NMR of Proteins and Nucleic Acids, Wiley, New YorK, 1986.
[26] M. Kjaergaard, S. Brander, F.M. Poulsen, Random coil chemical shift for intrinsically disordered proteins: effects of temperature and pH, J. Biomol. NMR 49(2) (2011) 139-149.

[27] R. Koradi, M. Billeter, K. Wuthrich, MOLMOL: a program for display and analysis of macromolecular structures, J. Mol. Graph. 14(1) (1996) 51-55.
[28] D.S. Wishart, B.D. Sykes, F.M. Richards, Relationship between nuclear magnetic resonance chemical shift and protein secondary structure, J. Mol. Biol. 222(2) (1991) 311-333.
[29] D.S. Wishart, B.D. Sykes, F.M. Richards, The chemical shift index: a fast and simple method for the assignment of protein secondary structure through NMR spectroscopy, Biochemistry 31(6) (1992) 1647-1651.
[30] L.A. Kelley, S.P. Gardner, M.J. Sutcliffe, An automated approach for clustering an ensemble of NMR-derived protein structures into conformationally related subfamilies, Protein Eng. Des. Sel. 9(11) (1996) 1063-1065.
[31] E.F. Pettersen, T.D. Goddard, C.C. Huang, G.S. Couch, D.M. Greenblatt, E.C. Meng, T.E. Ferrin, UCSF Chimera--a visualization system for exploratory research and analysis, J. Comput. Chem. 25(13) (2004) 1605-1612.
[32] J.E. Mills, P.M. Dean, Three-dimensional hydrogen-bond geometry and probability information from a crystal survey, J. Comput. Aided Mol. Des. 10(6) (1996) 607-622.
[33] D.S. Wishart, B.D. Sykes, F.M. Richards, Simple techniques for the quantification of protein secondary structure by 1H NMR spectroscopy, FEBS Lett. 293(1-2) (1991) 72-80.
[34] M. Pellecchia, B. Becattini, K.J. Crowell, R. Fattorusso, M. Forino, M. Fragai, D. Jung, T. Mustelin, L. Tautz, NMR-based techniques in the hit identification and optimisation processes, Expert Opin. Ther. Targets 8(6) (2004) 597-611.
[35] J. Amato, L. Cerofolini, D. Brancaccio, S. Giuntini, N. Iaccarino, P. Zizza, S. Iachettini, A. Biroccio, E. Novellino, A. Rosato, M. Fragai, C. Luchinat, A. Randazzo, B. Pagano, Insights into telomeric G-quadruplex DNA recognition by HMGB1 protein, Nucleic Acids Res. 47(18) (2019) 9950-9966.
[36] A. Singh, S. Khatun, A. Nath Gupta, Simultaneous Detection of Tyrosine and Structure-Specific Intrinsic Fluorescence in the Fibrillation of Alzheimer's Associated Peptides, Chemphyschem 21(23) (2020) 2585-2598.
[37] D. Florio, C. Di Natale, P.L. Scognamiglio, M. Leone, S. La Manna, S. Di Somma, P.A. Netti, A.M. Malfitano, D. Marasco, Self-assembly of bio-inspired heterochiral peptides, Bioorg. Chem. 114 (2021) 105047.
[38] M. Arias, K.B. Piga, M.E. Hyndman, H.J. Vogel, Improving the Activity of Trp-Rich Antimicrobial Peptides by Arg/Lys Substitutions and Changing the Length of Cationic Residues, Biomolecules 8(2) (2018).
[39] Y.X. Ma, A.F. Yao, X.L. Chen, L. Wang, C.B. Ma, X.P. Xi, T.B. Chen, C. Shaw, M. Zhou, Generation of truncated derivatives through in silico enzymatic digest of peptide GV30 target MRSA both in vitro and in vivo, Comput. Struct. Biotechnol. J. 19 (2021) 4984-4996.
[40] H. Miao, E. Burnett, M. Kinch, E. Simon, B. Wang, Activation of EphA2 kinase suppresses integrin function and causes focal-adhesion-kinase dephosphorylation, Nat. Cell Biol. 2(2) (2000) 62-9.
[41] A. Petty, E. Myshkin, H. Qin, H. Guo, H. Miao, G.P. Tochtrop, J.T. Hsieh, P. Page, L. Liu, D.J. Lindner, C. Acharya, A.D. MacKerell, Jr., E. Ficker, J. Song, B. Wang, A small molecule agonist of EphA2 receptor tyrosine kinase inhibits tumor cell migration in vitro and prostate cancer metastasis in vivo, PLoS One 7(8) (2012) e42120.
[42] R.M. Sharrard, N.J. Maitland, Regulation of protein kinase B activity by PTEN and SHIP2 in human prostate-derived cell lines, Cell. Signal. 19(1) (2007) 129-38.
[43] C. Di Natale, C.F. Natale, D. Florio, P.A. Netti, G. Morelli, M. Ventre, D. Marasco, Effects of surface nanopatterning on internalization and amyloid aggregation of the fragment 264-277 of Nucleophosmin 1, Colloids Surf. B Biointerfaces 197 (2021) 111439.
[44] R. Joshi, L. Qin, X. Cao, S. Zhong, C. Voss, W. Min, S.S.C. Li, DLC1 SAM domain-binding peptides inhibit cancer cell growth and migration by inactivating RhoA, J. Biol. Chem. 295(2) (2020) 645-656.

[45] D. Gang, D.W. Kim, H.S. Park, Cyclic Peptides: Promising Scaffolds for Biopharmaceuticals, Genes (Basel) 9(11) (2018).
[46] C. Griesinger, G. Otting, K. Wuthrich, R.R. Ernst, Clean TOCSY for proton spin system identification in macromolecules, J. Am. Chem. Soc. 110 (1988) 7870-7872.
[47] A. Kumar, R.R. Ernst, K. Wuthrich, A two-dimensional nuclear Overhauser enhancement (2D NOE) experiment for the elucidation of complete proton-proton cross-relaxation networks in biological macromolecules, Biochem. Biophys. Res. Commun. 95(1) (1980) 1-6.
[48] U. Piantini, O.W. Sorensen, R.R. Ernst, Multiple quantum filters for elucidating NMR coupling networks, J. Am. Chem. Soc. 104 (1982) 6800-6801.
[49] T.L. Hwang, A.J. Shaka, Water suppression that works. Excitation sculpting using arbitrary waveforms and pulsed field gradients, J. Magn. Reson. Ser. A 112 (1995) 275-279.
[50] C. Bartels, Xia, T., Billeter, M., Güntert, P. & Wüthrich, K, The program XEASY for computer-supported NMR spectral analysis of biological macromolecules, J. Biomol. NMR 6(1) (1995) 1-10.
[51] T. Herrmann, P. Guntert, K. Wuthrich, Protein NMR structure determination with automated NOE assignment using the new software CANDID and the torsion angle dynamics algorithm DYANA, J. Mol. Biol. 319(1) (2002) 209-227.
[52] R.A. Laskowski, J.A. Rullmannn, M.W. MacArthur, R. Kaptein, J.M. Thornton, AQUA and PROCHECK-NMR: programs for checking the quality of protein structures solved by NMR, J. Biomol. NMR 8(4) (1996) 477-486.
[53] L. Hellinen, S. Bahrpeyma, A.K. Rimpela, M. Hagstrom, M. Reinisalo, A. Urtti, Microscale Thermophoresis as a Screening Tool to Predict Melanin Binding of Drugs, Pharmaceutics 12(6) (2020).

Formatted: Font: 12 pt

Formatted: Font: (Default) Times New Roman, 12 pt

Formatted: Font: (Default) Times New Roman, 12 pt

Declaration of interests

☒ The authors declare that they have no known competing financial interests or personal relationships that could have appeared to influence the work reported in this paper.

☐The authors declare the following financial interests/personal relationships which may be considered as potential competing interests: